ARMINSKI, LESLIE MAXIMILIAN OTTO

THE TRANSPORT OF MACROMOLECULES ACROSS THE VASCULAR ENDOTHELIUM

City University of New York PH.D. 1980

THE TRANSPORT OF MACROMOLECULES ACROSS THE VASCULAR ENDOTHELIUM

by

Leslie Arminski

A dissertation submitted to the Graduate Faculty in Engineering in partial fulfillment of the requirements for the degree of Doctor of Philosophy, The City University of New York.

1980

This manuscript has been read and accepted for the Graduate Faculty in Engineering in satisfaction of the dissertation requirement for the degree of Doctor of Philosophy.

1/25/80
date

Chairman of Examining Committee

1/25/80
date

Executive Officer

Prof. Latif M. Jiji

Prof. Robert Pfeffer, Chairman

Prof. Sheldon Weinbaum

Prof. Herbert Weinstein

Supervisory Committee

The City University of New York

Abstract

THE TRANSPORT OF MACROMOLECULES ACROSS
THE VASCULAR ENDOTHELIUM

by

Leslie Arminski

Adviser: Professor Robert Pfeffer
Co-Adviser: Professor Sheldon Weinbaum

The subject of this thesis is the vesicular transport of macromolecules across vascular endothelium. In chapter I the dynamics of a Brownian collision is studied so that some insight can be gained on the displacement of a vesicle involved in a thermal collision with a large intracellular protein or a water molecule. New analytic solutions to the continuum hydrodynamic equations for the transient response of a spherical particle at low Reynolds number to several simple excitation forces $\vec{f}(t)$ of varying duration and different waveforms are presented. The new solutions permit the exploration of the effect of the waveform and the duration of impulse on the relative magnitudes of the inertia, quasi-steady Stokes' drag and unsteady boundary layer (Basset) force components throughout the time history of the motion. It is shown that for an impulse of constant magnitude the net displacement of the particle is independent of both the duration and waveform of the excitation force.

This simple result is used to explain why one obtains the correct Stokes-Einstein expression for the infinite time diffusion coefficient from a traditional Langevin analysis in which, historically, an incorrect quasi-steady linear Stokes resistance law has been used. The fluctuation of a vesicle due to an individual thermal collision is also shown to be of order 0.05 nm or less.

In chapter II the steady state hydro-electrodynamic model of Weinbaum and Caro (1976) for the vesicular transport of macromolecules across endothelial cell layers is extended to unsteady quasi one-dimensional vesicle diffusion and applied to existing time dependent vesicle labelling studies. The model accounts for the spatially varying hydrodynamic and van der Waals force interaction between the vesicle and the boundary plasmalemma membranes of the endothelial cell. It is also shown how Rubin's (1977) combined diffusion-reaction kinetics model for steady state permeability can be generalized to include an arbitrary spatial variation of the diffusion coefficient for a variable hydrodynamic resistance law in the cell interior. Approximate time dependent solutions, valid for all times, are obtained using a novel integral solution technique for a multilayered media with variable diffusivity. Dimensionless time dependent concentration profiles and flux ratios and dimensionless steady state permeability coefficients are generated independent of the cytoplasmic viscosity. When the time dependent tracer data of Casley-Smith and

Chin (1971) is used the cytoplasmic viscosity is estimated to be 8.9 poise.

The time dependent theory of chapter II for the vesicular transport of macromolecules across endothelial cell layers is modified to include the effects of steric hindrance in chapter III. The spatial variation of the diffusion coefficient near the plasmalemma membranes of an endothelial cell layer is determined experimentally by measuring velocities of spheres settling under gravity perpendicular to a single plate fitted with an array of attached spheres that model the ultrastructural features of a plasma membrane and its attached vesicles. The spatial variation of the diffusion coefficient in the central part of the cell is determined by the recent hydrodynamic theory of Ganatos, Weinbaum and Pfeffer (1979) for the creeping motion of a sphere between two plane parallel walls. This improved description of the vesicle dynamics is used to generate concentration profiles using the theoretical formulation of chapter II and compared with the time dependent tracer data of Casley-Smith and Chin (1971). When the data of Casley-Smith and Chin is used it is estimated that the cytoplasmic viscosity is in a range of 6.4-8.5 poise.

ACKNOWLEDGEMENTS

I wish to thank Professor Robert Pfeffer and Professor Sheldon Weinbaum for their continuous guidance and many contributions in directing this research. I also wish to thank Mr. Jonah Smith for performing the experimental runs reported in chapter III, Mr. John Da Silva, Artist in Residence at the Leonard Davis Center for Performing Arts (Picker Film Institute) for his assistance in lighting of the experiment, Messrs. William Hall and John Bodnaruk who built the experimental apparatus and the City University of New York Computer Center for the use of their facilities.

This research was sponsored by the National Science Foundation under Grant no. ENG 75-19243 and the National Institutes of Health under Grant no. HL 19454. Their support is gratefully acknowledged.

TABLE OF CONTENTS

LIST OF TABLES

LIST OF FIGURES

PHYSIOLOGICAL BACKGROUND

PHYSIOLOGICAL BACKGROUND

Electron microscopic (Karnovsky, 1967; Simionescu, Simionescu and Palade, 1973) and perfusion (Fry, 1972; Siflinger, Caro and Parker, 1975; Caro, 1978) studies have shown that the endothelial cell layer is the rate limiting barrier in the transport of macromolecules across the arterial wall. As first hypothesized by Palade (1960) and subsequently confirmed by Casley-Smith and Chin (1971) and Simionescu, Simionescu and Palade (1973) using electron dense tracers, macromolecules with dimensions greater than roughly 20 to 40 Å, depending on the particular junctional complex, cross the endothelial cell layer primarily by vesicular transport.

Vesicles are spherical, 700 Å, membrane bound intracellular bound bodies. It is postulated from electron micrographic (Palade and Bruns, 1968) and other observations that the vesicle transport process involves the following stages:

a) Stage of attached vesicle. Transmission electron micrographs of the peripheral zone of arterial endothelium show a large number of vesicles are attached to both the luminal and abluminal plasmalemmal membranes. During the period that the vesicle is attached and open to the outside fluid, molecular diffusion will result in the composition of the fluid in the vesicle approaching that of the fluid outside. The time course will depend on such factors as temperature, appropriate bulk diffusion coefficient and especially for

larger materials, the relative dimensions of the vesicular neck and the diffusing species. Whether equilibrium concentration is achieved will depend on these factors and the length of time the vesicle remains attached and open.

b) Stage of vesicle detachment. After a period of being attached the vesicle becomes detached from the plasmalemma. The nature of this process is not fully understood. It probably involves a molecular level disruption of the membrane bilayer in the neck, a sealing of the vesicle as well as the plasmalemma and the disappearance of the vesicle stalk by which it is attached to the plasmalemma. Since electron microscopic studies rarely show the detachment stage it is presumed that its duration is much shorter than that of either open attachment or transendothelial diffusion.

c) Stage of vesicle diffusion. Once detached from the plasmalemma membrane, the vesicle undergoes a diffusional migration across the cell which is strongly influenced by a hydrodynamic and molecular force interaction with the plasmalemma membranes of the endothelial cell and to a lesser extent by the interaction with other vesicles.

d) Stage of vesicle attachment. When the vesicle arrives in the vicinity of the plasmalemma (about 200 Å), molecular interaction forces (probably of van der Waals origin) arise between the opposing membranes. Electron microscopic studies (Palade and Bruns, 1968) have shown indentation of the plasmalemma facing a nearby vesicle followed by a flattening of opposing

plasmalemma and vesicle membranes over a distance of 300-400 Å. These findings suggest the existence of strong attractive forces between the membranes. The transition from the 'contact configuration' to the 'attached configuration' is thought to involve membrane breakdown in the middle of the contact area and membrane fusion in the rim of this area leading to the formation of a vesicle neck. The diaphragm, which ultimately disappears, may while present interfere with the loading of vesicles. Since the attachment process is seldom seen in electron micrographs, it is presumed that its duration, like that of the detachment process, is considerably shorter than the duration of the stage of attachment.

The processes described above are believed to apply to vesicles on both the luminal and abluminal fronts of endothelial cells (Simionescu, Simionescu and Palade, 1976). The repeated occurence of this sequence makes possible the transport of macromolecules across the cell.

To get a better understanding of the stage of diffusion and the stage of vesicle detachment the following research will be considered. In chapter I the dynamics of a Brownian collision is studied so that some insight can be gained on the displacement of a vesicle involved in a thermal collision with a large intracellular protein or water molecule. Chapter II investigates time dependent labelling of the endothelial cell layer and chapter III looks at the effect of steric hindrance due to attached plasmalemmal vesicles on the vesicular transport process.

CHAPTER I

EFFECT OF WAVEFORM AND DURATION OF IMPULSE ON THE SOLUTION TO THE BASSET-LANGEVIN EQUATION

I-1. INTRODUCTION

It is unclear whether the detachment of a vesicle is triggered by an individual collision with a large intracellular particle, or due to the collective behavior on a larger time scale of numerous collisions with water molecules in which the vesicle membrane experiences large amplitude deformations. There is also a lack of knowledge on the total displacement of a vesicle during an individual collision and on the time scale over which this occurs. To obtain insight into these problems a basic study of the dynamics of a Brownian collision will be undertaken in chapter I.

An analytic study of the transient response of a spherical particle at very low Reynolds number to several idealized excitation forces of different waveform and arbitrary duration will be presented. Previous analytic solutions of the Basset equation (also referred to as the Basset-Boussinesq-Oseen equation) have either been for a constant force of infinite duration (Villat, 1943) or delta function impulse (Hinch, 1975). The results for the top hat and single saw tooth forcing functions presented herein provide a qualitative picture of the transition in behavior that occurs between these two limiting cases of zero and infinite duration in addition to showing the effect of the waveform.

These simple forcing functions can be used as idealized models to study the dynamics of a Brownian collision or the response of a microhydrodynamic particle to a turb-

ulent fluid fluctuation. An application of particular interest is the amplitudes of the various forces on membrane bound bodies (vesicles) inside biological cells when subject to thermal collisions with other intracellular particles of various dimensions. In calculating the membrane elastic stresses generated it is important to distinguish between a volume force such as inertia and a steady or unsteady surface stress, Stokes and Basset forces, respectively. This work is the first to examine, in detail, the individual surface and volume forces throughout the time history of the motion for an applied force of finite duration.

In applying the present analysis to the motion of a Brownian particle, one assumes a governing equation, as first proposed by Langevin, of the form

$$m'(d\vec{u}/dt)+\vec{F}=\vec{f}(t) \ , \qquad (I.1)$$

where the force on a particle of mass m' and instantaneous velocity $\vec{u}$ can be partitioned into a slowly varying hydrodynamic force $\vec{F}$ due to the collective behavior of all neighboring molecules and a rapidly fluctuating force $\vec{f}(t)$ due to individual thermal collisions where $\vec{f}(t)$ is a stationary random function of time whose magnitude is determined by the equipartition of energy at thermodynamic equilibrium.

The validity of the Langevin equation and the deriva-

tion of the velocity correlation function $A(t) = \langle \vec{u}(t) \cdot \vec{u}(0) \rangle$ for the relaxation of a Brownian particle based on this equation have been the subject of considerable interest recently since the computer simulation experiments (Alder and Wainwright, 1967, 1968) with hard spheres first demonstrated that A(t) exhibited an asymptotic $t^{-3/2}$ decay. In classical Langevin theory, where a quasi-steady Stokes' resistance law linear in the instantaneous velocity is used for $\vec{F}$, one obtains an exponential decay. Numerical solutions of the time dependent Navier-Stokes equations (Alder and Wainwright, 1970) and asymptotic solutions of the unsteady Stokes creeping motion equation for large time using a generalized frequency dependent friction coefficient (Zwanzig and Bixon, 1970) or linear response theory (Widom, 1971) have since confirmed the $t^{-3/2}$ decay for A(t) and have shown that the discrepancy in the behavior of the velocity correlation function is due to the use of an incomplete resistance law for the drag on a particle in time dependent motion at low Re.

The correct expression for the hydrodynamic drag on a particle, first attributed to Basset (1888) and derived more recently using Fourier transform analysis (Landau and Lifshitz, 1959), shows that $\vec{F}$ is the linear superposition of three components, an instantaneous quasi-steady Stokes' drag, a virtual mass force due to the kinetic energy of the surrounding fluid, and a force relating to the time history of the past acceleration of

the particle (Basset force). The latter force arises from the unsteady velocity boundary layer at the surface of the particle and the modification of the external pressure field due to the displacement effect of this boundary layer.

An important question that has still not been completely resolved is why the expression for the infinite time particle diffusivity

$$D = \lim_{t\to\infty} \frac{1}{2}\frac{d}{dt}\langle \vec{x}(t)\cdot\vec{x}(t)\rangle = \int_0^\infty \langle \vec{u}(t)\cdot\vec{u}(0)\rangle dt \qquad (I.2)$$

derived using the incorrect resistance formula yields the same result

$$D = \kappa T \zeta^{-1}, \qquad (I.3)$$

as obtained by Einstein (1905) using an equilibrium thermodynamic approach that is not marred by these inconsistencies in the resistance law for unsteady flow. In Eq. (I.3), κ is Boltzmann's constant, T is the temperature, and ζ is the hydrodynamic friction tensor. Batchelor (1976) suggests that the explanation lies in the fact that the formal relation for D, Eq. (I.2), is also $2\pi\Psi(0)$, where $\Psi(0)$ is the zero frequency component of the Fourier transform of the velocity correlation function. The integral of Eq. (I.2) is, except for a constant factor, the mean square displacement of the particle and thus

$[\psi(0)/t]^{1/2}$ in the limit $t \to \infty$ is proportional to an average diffusion velocity over the total particle displacement. Batchelor then argues that the dominant contribution to this displacement comes from the nearly quasi-steady low frequency components of the motion. This, however, does not explain the paradox since the present results show that the neglected Basset force is of comparable magnitude to the quasi-steady Stokes' drag during the asymptotic portion of the velocity decay where one would expect an almost quasi-steady motion to exist.

There is no simple relation between these Fourier spectral arguments advanced by Bactchelor for a random forcing and the solution of the deterministic equation (I.1). However, if the forcing is a stationary random function of time, the relaxation of the test particle can be determined from (I.1) where the averaging is performed over all initial conditions on the velocity. In view of these remarks, it is interesting that the exact solutions of Eq. (I.1) presented here show that the dominant contributions to the displacement of a particle in an individual collision do not arise from the asymptotic decay of the velocity field for large time where the particle motion is of a quasi-steady character. This paradox will be explained for the infinite time diffusivity by integrating the full equation of motion and showing that the integral of the previoulsy neglected Basset force is zero for any motion that starts at rest and ends at rest.

I-2. BASIC EQUATION SINGLE SPHERE

The governing equation for the arbitrary motion of an isolated sphere of radius a and density ρ_s in an incompressible stationary viscous field of density ρ and viscosity μ at low Re is (Basset, 1888)

$$\frac{4}{3}\pi a^3 \rho_s \frac{d\vec{u}}{dt} = \frac{4}{3}\pi a^3(\rho_s-\rho)\vec{g} - 6\pi\mu\vec{u}a - \frac{1}{2}\frac{4}{3}\pi\rho a^3\frac{d\vec{u}}{dt}$$

$$- 6(\pi\rho\mu)^{1/2}a^2\int_0^t \frac{d\vec{u}}{d\tau}\frac{d\tau}{(t-\tau)^{1/2}} + \vec{f}(t), \quad \text{(I.4)}$$

where t is time and $\vec{g}$ is the gravitational acceleration. The forces on the right-hand side of Eq. (I.4) are the buoyancy force, quasi-steady Stokes' drag, fluid inertia or virtual mass force, Basset force, and the forcing function $\vec{f}(t)$. The vector Eq. (I.4) can also be written for any scalar velocity component. Equation (I.4) is also the incompressible Langevin Equation (I.1) for a single particle.

An equation very similar to Eq. (I.4) has been proposed by Tchen (1947) to describe the motion of a discrete particle interacting with a turbulent fluid eddy. The approximate equation for the motion of the particle given in Tchen is

$$\frac{4}{3}\pi a^3 \rho_s \frac{d\vec{u}}{dt} = \frac{4}{3}\pi a^3(\rho_s-\rho)\vec{g} + 6\pi\mu a\vec{w} + \frac{1}{2}\pi a^3\rho\frac{d\vec{w}}{dt}$$

$$+ 6(\pi\rho\mu)^{1/2}a^2\int_0^t \frac{d\vec{w}}{d\tau}\frac{d\tau}{(t-\tau)^{1/2}} + \frac{4}{3}\pi a^3\rho\frac{d\vec{v}}{dt}, \quad \text{(I.5)}$$

where $\vec{w}$ is the local relative velocity $\vec{v} - \vec{u}$ between fluid eddy and the particle. The right-hand side of Eq. (I.5) is seen by comparison with (I.4) to be the linear superposition of the force due to the instantaneous relative motion $\vec{w}$ and an inertial force due to the pressure interaction between the local eddy motion and the displaced fluid volume of the spherical particle. The limitations on the validity of Eq. (I.5) are discussed in Corrsin and Lumley (1956) and Hinze (1975).

Equations (I.4) and (I.5) are conveniently nondimensionalized by introducing the following scaled variables:

$$\tilde{\rho} = \frac{\rho_s}{\rho}, \quad t^* = \frac{t}{\rho a^2/\beta\mu}, \quad \vec{u}^* = \frac{\vec{u}}{u_0}$$

$$\vec{w}^* = \frac{\vec{w}}{u_0}, \quad \beta = \frac{9}{2}\left(\tilde{\rho} + \frac{1}{2}\right)^{-1}, \tag{I.6}$$

where $\rho a^2/\beta\mu$ is a Stokes' relaxation time t_s and u_0 is the mean thermal velocity associated with the translational kinetic energy of the particle plus its added fluid inertia. The dimensionless form of Eq. (I.4) is

$$\frac{d\vec{u}^*}{dt^*} + \vec{u}^* + \left(\frac{\beta}{\pi}\right)^{1/2} \int_0^{t^*} \frac{d\vec{u}^*}{d\tau} \frac{d\tau}{(t^*-\tau)^{1/2}}$$

$$= \frac{2}{9}\left(\tilde{\rho} - 1\right)\frac{a^2\vec{g}}{\nu u_0} + \frac{\vec{f}(t^*)}{6\pi a \mu u_0}, \tag{I.7}$$

where ν is the kinematic viscosity. Equation (I.5), after

a simple regrouping of terms, becomes

$$\frac{d\vec{w}^*}{dt^*} + \vec{w}^* + \left(\frac{\beta}{\pi}\right)^{1/2} \int_0^{t^*} \frac{d\vec{w}^*}{d\tau} \frac{d\tau}{(t^*-\tau)^{1/2}}$$

$$= -\frac{2}{9}(\tilde{\rho}-1)\frac{a^2\vec{g}}{\nu u_0} + \frac{2}{9}(\tilde{\rho}-1)\frac{d\vec{v}^*}{dt^*} \quad , \qquad \text{(I.8)}$$

The Basset-Langevin equation (I.7) or the Tchen equation (I.8) written in the relative velocity $\vec{w}^*$ are thus seen to be of identical mathematical form, with the fluid eddy acceleration $d\vec{v}^*/dt^*$ playing the same role as the thermal collision force $\vec{f}(t^*)$. In the present study $d\vec{v}^*/dt^*$ will be treated as if it were a Lagrangian derivative whose time dependence is specified. Thus, the entire right-hand side of Eqs. (I.7) and (I.8) will be considered a known but arbitrary function of time, $\vec{F}(t^*)$.

In accord with the foregoing remarks, a solution of the linear integrodifferential equation (asterisk dropped)

$$\frac{du}{dt} + u + \left(\frac{\beta}{\pi}\right)^{1/2} \int_0^t \frac{du}{d\tau} \frac{d\tau}{(t-\tau)^{1/2}} = F(t) \quad , \qquad \text{(I.9)}$$

is sought, where F(t) is defined by the appropriate scalar component of Eqs. (I.7) or (I.8) and $u(t) = 0$ for $t < 0$. Several different approaches have been developed for treating Eq. (I.9). Widom (1971) uses a linear response theory described in Kubo (1966) and Berne (1971). Zwanzig and Bixon (1970) employ a frequency dependent friction tensor while Hinze (1975) describes a Fourier integral

transform technique. It is found, however, that the most convenient procedure for obtaining analytic solutions to (I.9) for simple forms of F(t) is to first convert Eq. (I.9) to a second order constant coefficient linear differential equation using Abel's integral identity

$$\pi[u(t)-u(0)] = \int_0^t \frac{1}{\sqrt{t-t'}} \int_0^{t'} \frac{du}{d\tau} \frac{d\tau}{\sqrt{t'-\tau}} d\tau dt', \qquad \text{(I.10)}$$

and then solve this equation by variation of parameters. This solution procedure is described in Yih (1969) for a constant f(t). The more general formal solution for an arbitrary f(t) is presented in Tchen (1947). For a particle which is at rest for $t < 0$ and subject to an arbitrary F(t) for $t \geq 0$, this solution can be written in the form

$$u(t) = \frac{F(0)}{[\beta(\beta-4)]^{1/2}} [\exp(m_1 t) - \exp(m_2 t)] + \frac{1}{[\beta(\beta-4)]^{1/2}} \times \int_0^t G(\tau)\{\exp[m_1(t-\tau)] - \exp[m_2(t-\tau)]\} d\tau \qquad \text{(I.11)}$$

where

$$G(t) = F + \dot{F} - \left(\frac{\beta}{\pi}\right)^{1/2} \int_0^t \frac{F'(\tau)}{(t-\tau)^{1/2}} d\tau - \left(\frac{\beta}{\pi t}\right)^{1/2} F(0)$$

and

$$m_{1,2} = \frac{\beta}{2} - 1 \pm \left[\beta\left(\frac{\beta}{4} - 1\right)\right]^{1/2},$$

the subscripts 1,2 applying to the plus and minus radicals in that order. One notes that for $\beta > 4$ or $\tilde{\rho} < 5/8$, the roots m_i are real whereas for $\tilde{\rho} > 5/8$ the exponentials have complex arguments. The solution for u(t), Eq. (I.11), and its integral for the particle displacement x(t) are, except for a constant involving the mean thermal speed, the solution for the velocity correlation function $\langle \vec{u}(t) \cdot \vec{u}(0) \rangle$ and the time dependent diffusivity D(t) of a Brownian particle when u(t) is a stationary random function of time.

The integrals in Eq. (I.11) have heretofore only been evaluated analytically for the case where F(t) is constant throughout the motion. This case was studied by several early investigators (Basset, 1888, 1910; Boggio, 1907; Picciati, 1907; Villat, 1943) who were interested in the approach to a terminal settling velocity of a small particle released from rest in a gravitational field. The principal obstacle in applying Eq. (I.11) to other forcing functions is that the integrals are complex when $\tilde{\rho} > 5/8$ and difficult to evaluate for more complicated waveforms.

An important but simple result that can be derived directly from Eq. (I.9) is the net displacement of any particle which is accelerated from rest and eventually returns to rest as t approaches infinity.

Integrating Eq. (I.9) term by term from t = 0 to $t = \infty$, one finds that the integral of the inertia term

vanishes because of the end states on the velocity, the integral of the steady state Stokes' drag term is the net particle displacement, and that the integral of the Basset force term also vanishes after algebraic manipulations in which the Abel integral identity is employed. Thus,

$$X(\infty) = \int_0^\infty F(t)\,dt \,, \tag{I.12}$$

or the net particle displacement is equal to the total impulse in dimensionless form. This result is independent of the waveform of the external force. The fact that the Basset force does not contribute to the infinite time particle displacement is the reason that the correct expression for the infinite time diffusivity could be obtained from a traditional Langevin analysis in which an incorrect instantaneous linear resistance law was used. This interesting behavior has a simple physical interpretation. The Basset force arises from the diffusion of vorticity introduced or withdrawn at solid boundaries in the flow field. The vorticity conservation theorems state that the vorticity in the fluid cannot be destroyed but is redistributed by the action of viscosity (convection neglected for $Re \ll 1$). The simple solution for the arbitrary acceleration from rest of a flat plate parallel to itself shows that the amount of vorticity that enters the flow at the boundary depends only on the instantaneous velocity of the plate and that an

equal amount of vorticity re-enters the wall when the plate is brought back to rest. The net vorticity introduced in the fluid by a particle motion that starts at rest and ends at rest is thus zero.

I-3. SOLUTION OF EQ. (I.9) FOR PARTICULAR F(t)

The formal solution (I.11) is especially useful when the function G(t) in Eq. (I.11) can be evaluated in closed form and the integral terms (I.11) evaluated analytically. Two simple but instructive forcing functions F(t) for which these integrations can be performed are a constant force of finite duration and a linearly varying force of specified impulse. These two forcing functions provide a convenient pedagogical model to explore both the effect of waveform and duration of the applied force.

I-3a. Constant Force of Finite Duration

For this case one assumes

$$F(t) = K, \quad 0 \leq t \leq t_0 \tag{I.13a}$$

$$F(t) = 0, \quad t > t_0. \tag{I.13b}$$

The function G(t) in each interval is

$$G(t) = K\left[1 - \left(\frac{\beta}{\pi t}\right)^{1/2}\right], \quad 0 \leq t \leq t_0 \tag{I.14a}$$

$$G(t) = K\left\{\left[\frac{\beta}{\pi(t-t_0)}\right]^{1/2} - \left[\frac{\beta}{\pi t}\right]^{1/2}\right\}, \quad t > t_0. \tag{I.14b}$$

The solutions for u(t) are

$$\frac{u(t)}{K} = \left[1 + \left(\frac{m_2+1}{m_1-m_2}\right)\exp(m_1 t)\,\mathrm{erfc}(m_1 t)^{1/2} - \left(\frac{m_1+1}{m_1-m_2}\right)\exp(m_2 t)\,\mathrm{erfc}(m_2 t)^{1/2}\right], \quad 0 \leq t \leq t_0, \tag{I.15a}$$

$$\frac{u(t)}{K} = \left(\frac{m_2+1}{m_1-m_2}\right)\exp(m_1 t)\,\mathrm{erfc}(m_1 t)^{1/2} - \left(\frac{m_1+1}{m_1-m_2}\right)\exp(m_2 t)\,\mathrm{erfc}(m_2 t)^{1/2}$$

$$+\left(\frac{m_2+1}{m_1-m_2}\right)\exp[m_1(t-t_0)]\,\mathrm{erfc}[m_1(t-t_0)]^{1/2}$$

$$-\left(\frac{m_1+1}{m_1-m_2}\right)\exp[m_2(t-t_0)]\,\mathrm{erfc}[m_2(t-t_0)]^{1/2}, \quad t > t_0. \tag{I.15b}$$

Result (I.15a) is the previously mentioned solution for the acceleration from rest of a spherical particle under the action of a constant applied force of infinite duration. When $t_0 = 1/K$, the impulse of the external force is unity and the total displacement of the particle as $t \to \infty$ is $x(\infty) = 1$. The maximum velocity $u(t_0)$ achieved at the end of the acceleration phase, as shown later, decreases as t_0 increases starting with a maximum value of 1.0 for an impulsive collision.

To show the importance of the Basset force on the numerical results in Sec. I-4., given below are the equivalent solutions to Eqs. (I.15a) and (I.15b) that one obtains if the Basset force term is omitted in Eq. (I.9) and the same forcing equation (I.13) employed

$$u(t) = K\left[1 - \exp(-t)\right], \quad 0 \leq t \leq t_0 \tag{I.16a}$$

$$u(t) = K\left[1 - \exp(-t_0)\right]\exp\left[-(t - t_0)\right], \quad t > t_0. \tag{I.16b}$$

The solution for u(t) given by Eqs. (I.16) differs markedly from that given by Eqs. (I.15) and yet the area under each curve (the net particle displacement

as $t \to \infty$) is the same.

I-3b. Impulsive Force

The solution for an impulsive excitation force could be derived by introducing a Dirac delta function for F(t) in Eq. (I.11). A more convenient alternate approach is to take advantage of the solution for u(t) already obtained in (I.15b). One wishes to look at the limiting behavior in which $K \to \infty$ but $Kt_0 = 1$. The solution for u(t) is thus obtained by applying l'Hospital's rule

$$u(t) = \lim_{t_0 \to 0} \left(\frac{u(t)}{t_0} \right) = \lim_{t_0 \to 0} \frac{d\,u(t)}{d\,t_0} \,, \qquad \text{(I.17)}$$

where u(t) is the solution for a unit force on the right-hand side of Eq. (I.15b). Performing the differentiation indicated by Eq. (I.17), one finds, after some algebraic simplification, that

$$u(t) = \left(\frac{m_1 + 1}{m_1 - m_2} \right) \exp(m_1 t)\, \mathrm{erfc}(m_1 t)^{1/2} - \left(\frac{m_2 + 1}{m_1 - m_2} \right) \exp(m_2 t)\, \mathrm{erfc}(m_2 t)^{1/2} \qquad \text{(I.18)}$$

This solution, except for a multiplicative constant, is the velocity correlation function for an impulsive collision (last equation in Hinch (1975)).

I-3c. Single Saw Tooth Excitation Force

In order to explore the effect of the waveform of the

applied force, one can consider a simple linearly increasing forcing function of finite duration t_0:

$$F(t) = ct, \quad 0 \leq t \leq t_0, \tag{I.19a}$$

$$F(t) = 0, \quad t > t_0. \tag{I.19b}$$

The function G(t) in (I.11) for this case is

$$G(t) = c\left[t + 1 - 2\left(\frac{\beta}{\pi t}\right)^{1/2}\right], \quad 0 \leq t \leq t_0, \tag{I.20a}$$

$$G(t) = 2c\left(\frac{\beta}{\pi}\right)^{1/2}\left[(t-t_0)^{1/2} - \sqrt{t} + \frac{t_0}{2(t-t_0)^{1/2}}\right], \quad t > t_0. \tag{I.20b}$$

Substituting Eqs. (I.20) in (I.11) and evaluating the various integrals, one finds:

$$\begin{aligned}\frac{u(t)}{c} = t &- \frac{m_1(m_1+1)}{m_1 - m_2}\left[\exp(m_2 t)\,\mathrm{erfc}(m_2 t)^{1/2} + 2\left(\frac{m_2 t}{\pi}\right)^{1/2} - 1\right] \\ &+ \frac{m_2(m_2+1)}{m_1 - m_2}\left[\exp(m_1 t)\,\mathrm{erfc}(m_1 t)^{1/2} + 2\left(\frac{m_1 t}{\pi}\right)^{1/2} - 1\right], \quad 0 \leq t \leq t_0\end{aligned} \tag{I.21a}$$

$$\frac{u(t)}{c} = \frac{(m_1+1)(m_1+t_0)}{m_1-m_2}\,\mathrm{erfc}\left[m_2(t-t_0)\right]^{1/2}\exp\left[m_2(t-t_0)\right]$$

$$-\frac{(m_2+1)(m_2+t_0)}{m_1-m_2}\,\mathrm{erfc}\left[m_1(t-t_0)\right]^{1/2}\exp\left[m_1(t-t_0)\right]$$

$$+\frac{m_2(m_2+1)}{m_1-m_2}\,\mathrm{erfc}(m_1 t)^{1/2}\exp(m_1 t)$$

$$-\frac{m_1(m_1+1)}{m_1-m_2}\,\mathrm{erfc}(m_2 t)^{1/2}\exp(m_2 t)$$

$$+\frac{2m_2(m_2+1)}{m_1-m_2}\left\{\left[\frac{m_1 t}{\pi}\right]^{1/2}-\left[\frac{m_1(t-t_0)}{\pi}\right]^{1/2}\right\}$$

$$-\frac{2m_1(m_1+1)}{m_1-m_2}\left\{\left[\frac{m_2 t}{\pi}\right]^{1/2}-\left[\frac{m_2(t-t_0)}{\pi}\right]^{1/2}\right\}, \qquad \text{(I.21b)}$$

$$t > t_0.$$

For a unit impulse, F(t) must terminate at $t_0 = (2/c)^{1/2}$. From (I.12) the net displacement as $t \to \infty$ is $x(\infty) = 1$ independent of the value of c. The velocity u(t) and the individual forces, however, change dramatically as c is increased as discussed in Sec. I-4. In the limit as $c \to \infty$, one can show through the use of l'Hospital's rule, as just demonstrated for the finite duration constant force case, that the solution (I.21b) reduces to the impulsive excitation solution (I.18).

I-4. RESULTS AND DISCUSSION

A comparative study of the numerical results obtained from the analytic solutions for the various forcing functions in I-3 is presented in this section. I-4a compares the relative magnitudes of the individual forces acting on the sphere throughout the time history of its motion as a function of the waveform and duration of the applied force. I-4b describes the results for the velocity (velocity correlation function) and distance traveled (time dependent particle diffusivity) for a unit impulse.

I-4a. Comparison of Forces

To facilitate the presentation of results the governing equation of motion (I.9) will be written in the abbreviated notation

$$F_I + F_S + F_B = F(t), \tag{I.22}$$

Where F_I is the total inertial force of the particle plus surrounding fluid, F_S is the linear Stokes resistance, and F_B is the Basset force. For the acceleration phase of the motion, during which the excitation force F(t) is applied, it is convenient to divide (I.22) through by the instantaneous value of F(t) and write (I.22) as

$$\tilde{F}_I + \tilde{F}_S + \tilde{F}_B = 1 \tag{I.23}$$

where $\tilde{F}_I = F_I/F(t)$, $\tilde{F}_S = F_S/F(t)$, and $\tilde{F}_B = F_B/F(t)$. For the relaxation phase of the motion Eq. (I.23) is replaced by

$$\tilde{F}_I + \tilde{F}_S + \tilde{F}_B = 0 \qquad \text{(I.24)}$$

where each force is scaled by $F(t_0)$, the value of the external force at the instant it is removed. For the simplified analysis in which the Basset force is neglected, $\tilde{F}_B$ is set equal to zero in (I.23) and (I.24). This corresponds to the limiting case $\tilde{\rho} = \infty$. All the other solutions are for a neutrally buoyant particle $\tilde{\rho} = 1$ or $\beta = 3$. In the limit as $\tilde{\rho} \to 0$, β has its maximum value 9. Thus, the Basset force for a gas bubble [see Eq. (I.9)] is about 73 percent larger than the neutrally buoyant particle considered herein. $\tilde{F}_S$ is obtained from the analytic solution for u in the previous section, $\tilde{F}_I$ is found by differentiating these analytic solutions while $\tilde{F}_B$ is determined by substituting these results in Eqs. (I.23) or (I.24).

Figure I.1 shows the time history of the scaled forces during the acceleration phase for a constant and linearly increasing external force. Also shown in the figure is the solution for $\tilde{F}_B = 0$ based on result (I.16a). The external force which has been applied for up to 100 Stokes' relaxation times can be terminated at any smaller value $t = t_0$ to initiate the relaxation phase. It is evident that the inertial and Basset forces dominate the

early period of motion $t \ll 1$ and that for large times, $t \gg 10$ the principal forces are the Stokes' and Basset forces. By comparing the dashed and solid curves in this figure, one can obtain some feeling for the importance of the applied waveform on the magnitude of the individual force components.

Figures I.2 and I.3 illustrate the relaxation of the test particle for a forcing which is either short or long compared with a Stokes' relaxation time, $t_0 = 0.1$ and 10, respectively. The numerical results show that the duration of the applied force is more important than its detailed waveform. This is due to the slow build up of the linear Stokes' resistance for $t_0 \ll 1$ due to the much more rapid early growth of the Basset force. In many problems of interest and in particular for Brownian motion, the acceleration phase is terminated for values of $t_0 \ll\ll 1$. The linear Stokes' resistance force, which formed the basis for the traditional Langevin analysis, is thus seen to be small compared with the neglected Basset force at the end of the acceleration phase.

Table I.1 shows the results for the relaxation phase following a unit impulsive acceleration. The individual forces in this case have not been scaled since the applied force is infinite. The initial behavior $t \ll 0.2$ is dominated by the inertial and Basset forces. The long-time behavior $t \gg 10$ is controlled by a balance between F_S and F_B although both forces are very small. It is

this tail which gives rise to the $t^{-3/2}$ asymptotic decay of the velocity correlation function discussed in the introductory section. The intriguing numerical result is that the net particle displacement is not dominated by this asymptotic decay or the low frequency behavior of the velocity correlation function as suggested by Batchelor (1976). The particle has already traveled half of its total displacement when $t \approx 2.6$. Also, F_S and F_B are both small and of nearly equal magnitude for $t > 10$.

Figure I.2 is of special interest in light of the recent study (Weinbaum and Caro, 1976) of the vesicular transport inside endothelial cells. The time scale of the excitation force in this figure, $t_0 = 0.1$, is representative of what one would anticipate for the thermal collision of a large intracellular protein molecule with the vesicle. One observes from Figs. I.2 and I.3 that the inertia force is discontinuous and changes sign at $t = t_0$ whereas $\tilde{F}_S$ and $\tilde{F}_B$ are both continuous. The duration of the applied force has a dramatic effect on both the forces and instantaneous velocity of the particle, Figs. I.2, I.3, and I.4. When $t_0 = 0.1$ (a thermal collision with a particle smaller than the test particle), the quasi-steady Stokes' drag is not an important part of the motion until large times when all forces have decayed to small values and the motion is nearly over. The Basset force, which increases much more rapidly than the Stokes' resis-

tance, is the dominant hydrodynamic resistance even after the applied force is removed if the linear Stokes' resistance at the onset of the relaxation phase is small. When $t_0 >> 1$ (e.g., $t_0 = 10$ Fig. I.3), $\tilde{F}_B$ and $\tilde{F}_S$ are of comparable importance throughout the motion and much larger than the inertial force except for short times just after the onset and removal of the applied force.

I-4b. Velocity and Displacement for a Unit Impulse

Figures I.4, I.5, and I.6 show the solution for the velocity and particle displacement. Figures I.4 and I.5 show the effect of the duration of the applied force and its waveform on the velocity history of the particle for a unit impulse. It is evident from Fig. I.4 that the duration of the applied force for a fixed impulse has a profound effect on the maximum velocity achieved by the test sphere and hence on the entire velocity distribution. This occurs because an increasingly larger portion of the momentum imparted to the particle during the acceleration phase is dissipated by frictional resistance as t_0 increases. The waveform of the applied force, on the other hand, has a relatively modest influence on the velocity distribution, (see Fig. I.5).

The area under each of the curves in Fig. I.4 (distance traveled) is shown in Fig. I.6 for the constant forcing case. As already discussed, the total distance traveled by the test sphere during the acceleration and relaxation phases depends only on the total impulse imparted to

the sphere and is independent of both the duration and waveform of the external forcing. Thus, for a unit impulse all the curves in Fig. I.6 are asymptotic to 1.0. The ratio of the distance traveled during the interval that the external forcing is applied $x(t_0)$ to the total displacement $x(\infty)$ which is shown in Fig. I.7 for a constant force, is also primarily a function of t_0. For an impulsive forcing the entire displacement occurs during the relaxation phase whereas if t_0 approaches infinity $x(t_0)/x(\infty)$ approaches unity. Figure I.6 shows a striking difference in the behavior of the time dependent displacement of the test sphere depending on whether or not the Basset force is retained in the equation of motion (I.9). Without the Basset force present the approach to $x(\infty)$ is exponential, the value $x(t) = 0.99$ being achieved at $t \approx 5.0$. With the Basset force present the approach to $x(\infty)$ is as $t^{-1/2}$ the value $x(t) = 0.99$ being achieved at $t = O(10^4)$. It is clear from Fig. I.6 that the detailed memory of the initial forcing disappears on a time scale which is roughly one order of magnitude larger than the duration t_0 of the external forcing.

The distance traveled by a vesicle involved in a thermal collision can now be estimated. In dimensional form the distance traveled in time t is

$$X(t) = \int_0^t u \, dt \qquad (I.25)$$

Substituting relation (I.6) for u and t in (I.25) gives

$$x(t) = u_o t_s \int_o^{t^*} u^* \, dt^* \qquad \text{(I.26a)}$$

or

$$x(t) = u_o t_s x^*(t^*) \qquad \text{(I.26b)}$$

On the shortest time scale, that of molecular collision, the impulse force accelerates the vesicle to its random thermal velocity. If the vesicle is in thermodynamic equilibrium with its surroundings, the mean thermal speed of the vesicle u_0 after collision is given by $(3kT/m')^{1/2}$. The thermal speed at 37°C of a 700 Å vesicle whose density is that of water is roughly 30 cm/sec, where m' is taken as $\frac{4}{3}\pi \rho_s a^3$.

For a unit impulse external forcing, it is known from (I.12) that $x^*(\infty) = 1.0$. Thus the total distance traveled by the vesicle until it comes to rest is

$$x(\infty) = u_o t_s \qquad \text{(I.27)}$$

All the values for calculating t_s have been given previously except the intracellular viscosity μ of endothelial cells. There are at present no reliable measurements available for this physical quantity. Values in the literature span the range from 0.2 poise (Casley-Smith and Chin, 1971) to 8 poise (Shea, Karnovsky and Bossert, 1969) and higher. Thus, it is only possible to estimate the net vesicle displacement of a vesicle, using (I.27), due to a single thermal collision to be of order 0.05 nm or less.

Table I.1. Forces acting on a sphere, with velocity and distance traveled, in response to a Dirac delta function.

Time t	Velocity or Stokes drag u or F_S	Distance traveled x	Inertial force F_I	Basset force F_B
0.000	1.00	0.00	$-\infty$	∞
0.001	9.40×10^{-1}	9.60×10^{-4}	-2.90×10^{1}	2.80×10^{1}
0.002	9.16×10^{-1}	1.89×10^{-3}	-1.99×10^{1}	1.90×10^{1}
0.005	8.71×10^{-1}	4.56×10^{-3}	-1.20×10^{1}	1.11×10^{1}
0.010	8.23×10^{-1}	8.79×10^{-3}	-7.96	7.13
0.020	7.60×10^{-1}	1.67×10^{-2}	-5.17	4.41
0.050	6.49×10^{-1}	3.77×10^{-2}	-2.76	2.11
0.100	5.46×10^{-1}	6.73×10^{-2}	-1.61	1.07
0.200	4.29×10^{-1}	1.15×10^{-1}	-8.72×10^{-1}	4.43×10^{-1}
0.500	2.71×10^{-1}	2.16×10^{-1}	-3.28×10^{-1}	5.71×10^{-2}
1.000	1.67×10^{-1}	3.22×10^{-1}	-1.32×10^{-1}	-3.50×10^{-2}
2.000	9.01×10^{-2}	4.44×10^{-1}	-4.46×10^{-2}	-4.55×10^{-2}
5.000	3.25×10^{-2}	6.03×10^{-1}	-7.96×10^{-3}	-2.45×10^{-2}
10.000	1.33×10^{-2}	7.06×10^{-1}	-1.79×10^{-3}	-1.15×10^{-2}
20.000	5.06×10^{-3}	7.87×10^{-1}	-3.60×10^{-4}	-4.70×10^{-3}
50.000	1.34×10^{-3}	8.63×10^{-1}	-4.00×10^{-5}	-1.30×10^{-3}
100.000	4.81×10^{-4}	9.02×10^{-1}	-7.15×10^{-6}	-4.74×10^{-4}
1000.000	1.54×10^{-5}	9.69×10^{-1}	-2.31×10^{-8}	-1.54×10^{-5}
10000.000	4.89×10^{-7}	9.90×10^{-1}	-7.33×10^{-11}	-4.88×10^{-7}

CHAPTER I. NOMENCLATURE

a	particle radius
$A(t)$	time dependent velocity correlation function
c	slope of linear forcing function
$D(t)$	time dependent particle diffusivity
$\vec{f}(t)$	rapidly fluctuating force due to individual thermal collisions
$\vec{F}(t)$	slowly varying hydrodynamic force due to the collective behavior of all neighboring molecules
F_B	Basset force
F_I	total inertial force of the particle plus surrounding fluid
F_S	linear Stokes resistance
$\tilde{F}_B$	scaled force $\tilde{F}_B = F_B/F(t)$
$\tilde{F}_I$	scaled force $\tilde{F}_I = F_I/F(t)$
$\tilde{F}_S$	scaled force $\tilde{F}_S = F_S/F(t)$
$\vec{g}$	gravitational acceleration
$G(t)$	function defined by (I.11)
k	Boltzmann's constant
K	amplitude of constant forcing function
m'	mass
m_i	roots of indicial equation $m^2 + (2 - \beta) + 1 = 0$
Re	Reynolds number
t	time
t^*	scaled time $t^* = t/t_s$
t_0	end of acceleration phase
t_s	Stokes relaxation time $t_s = \rho a^2/\beta\mu$
T	temperature

$\vec{u}$	instantaneous velocity
$\vec{u}^*$	scaled velocity $\vec{u}^* = \vec{u}/u_0$
u_0	mean thermal velocity associated with the translational kinetic energy of the particle plus its added fluid inertia
$\vec{v}$	fluid eddy velocity
$\vec{v}^*$	scaled velocity $\vec{v}^* = \vec{v}/u_0$
$\vec{w}$	local relative velocity $\vec{w} = \vec{v} - \vec{u}$
$\vec{w}^*$	scaled velocity $\vec{w}^* = \vec{w}/u_0$
$\vec{x}$	distance coordinate
$\vec{x}^*$	scaled distance coordinate $\vec{x}^* = \vec{x}/u_0 t_s$
β	scaled density $\beta = \frac{9}{2}(\tilde{\rho} + \frac{1}{2})^{-1}$
ζ	hydrodynamic friction tensor
μ	viscosity
ν	kinematic viscosity
ρ	fluid density
$\tilde{\rho}$	scaled density $\tilde{\rho} = \rho_s/\rho$
ρ_s	particle density
$\psi(t)$	time dependent frequency component of Fourier transform of velocity correlation function

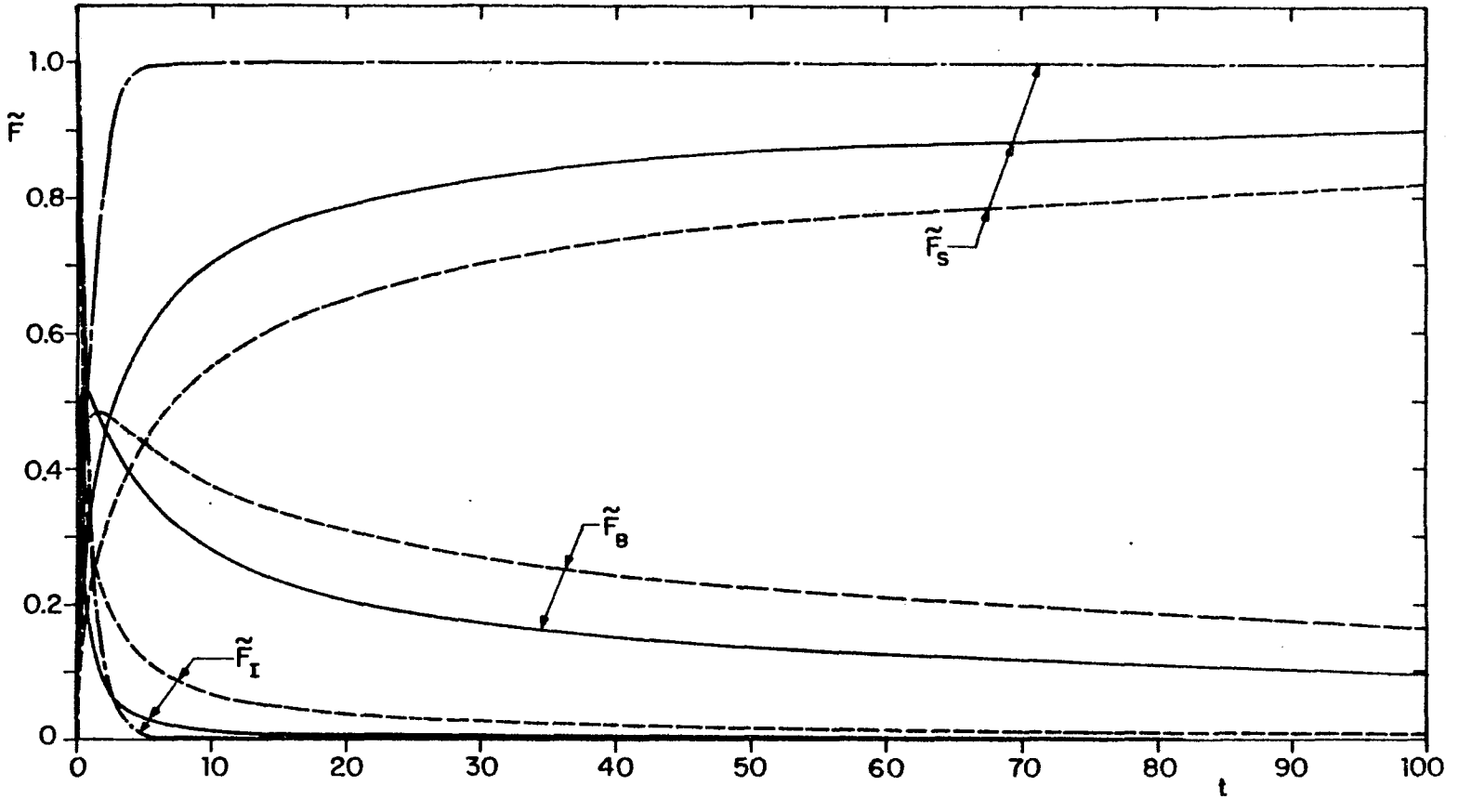

Figure I.1. Time history of scaled forces acting on a sphere during acceleration phase; —— constant force [Eq. (I.15a)] , ---- linear force [Eq. (I.21a)] , -•-•- constant force with $\tilde{F}_B = 0$ [Eq. (I.16a)] .

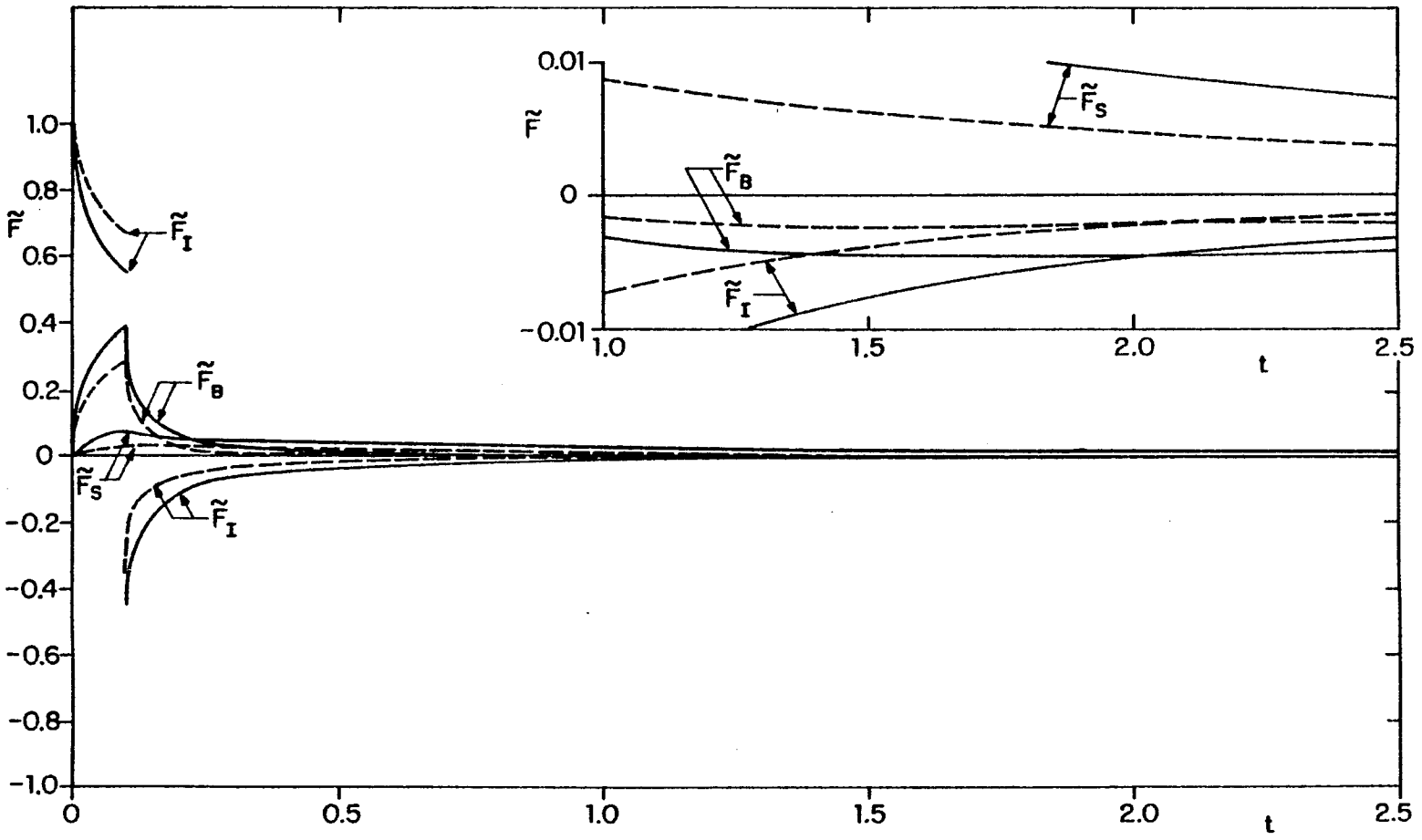

Figure I.2. Time history of scaled forces acting on a sphere in response to a unit impulse of duration $t_0 = 0.1$; —— constant force [Eqs. (I.15a) and (I.15b)], ---- linear force [Eqs. (I.21a) and (I.21b)].

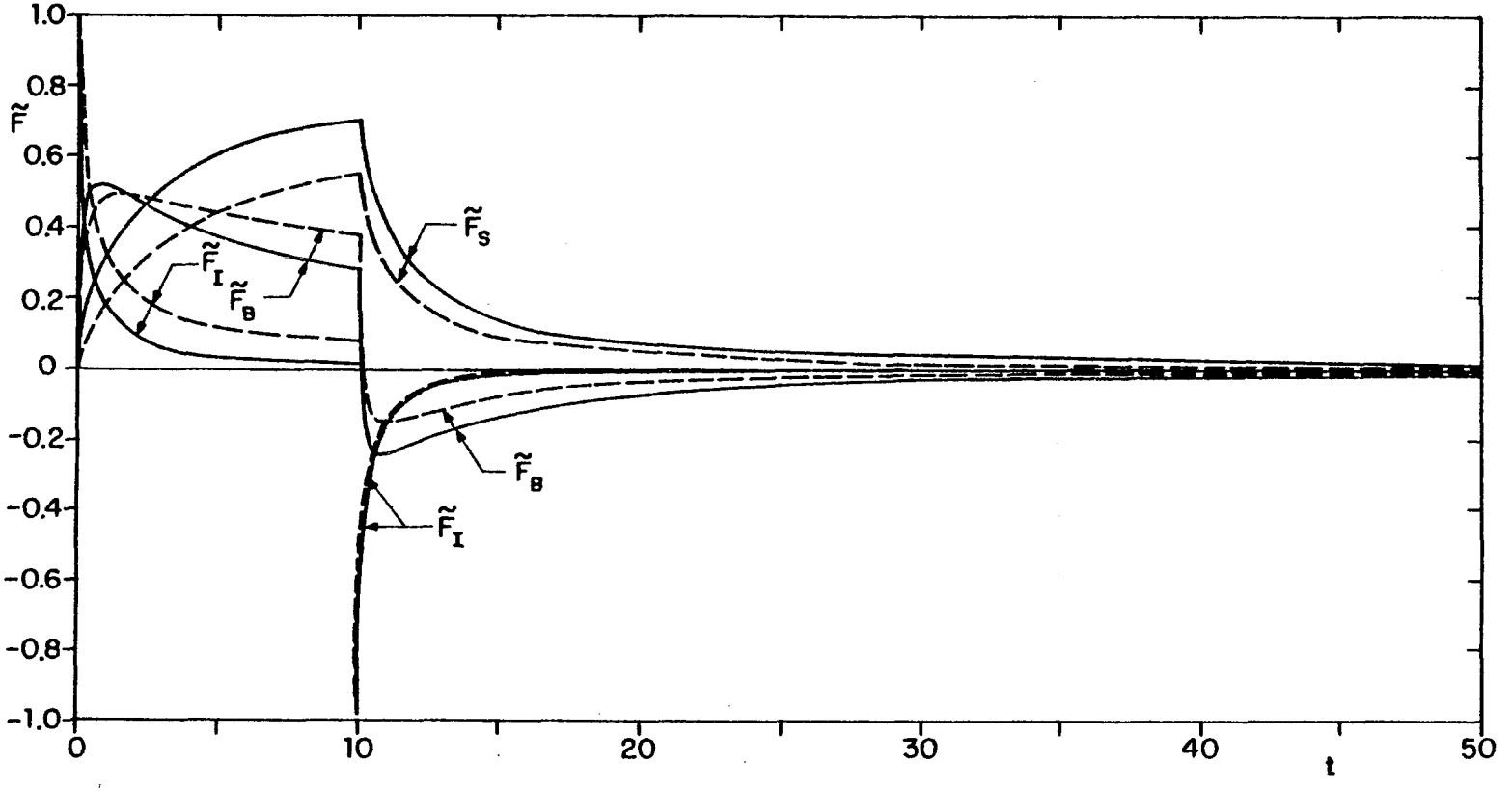

Figure I.3. Time history of scaled forces acting on a sphere in response to a unit impulse of duration $t_0 = 10.0$; —— constant force [Eqs. (I.15a) and (I.15b)], ---- linear force [Eqs. (I.21a) and (I.21b)].

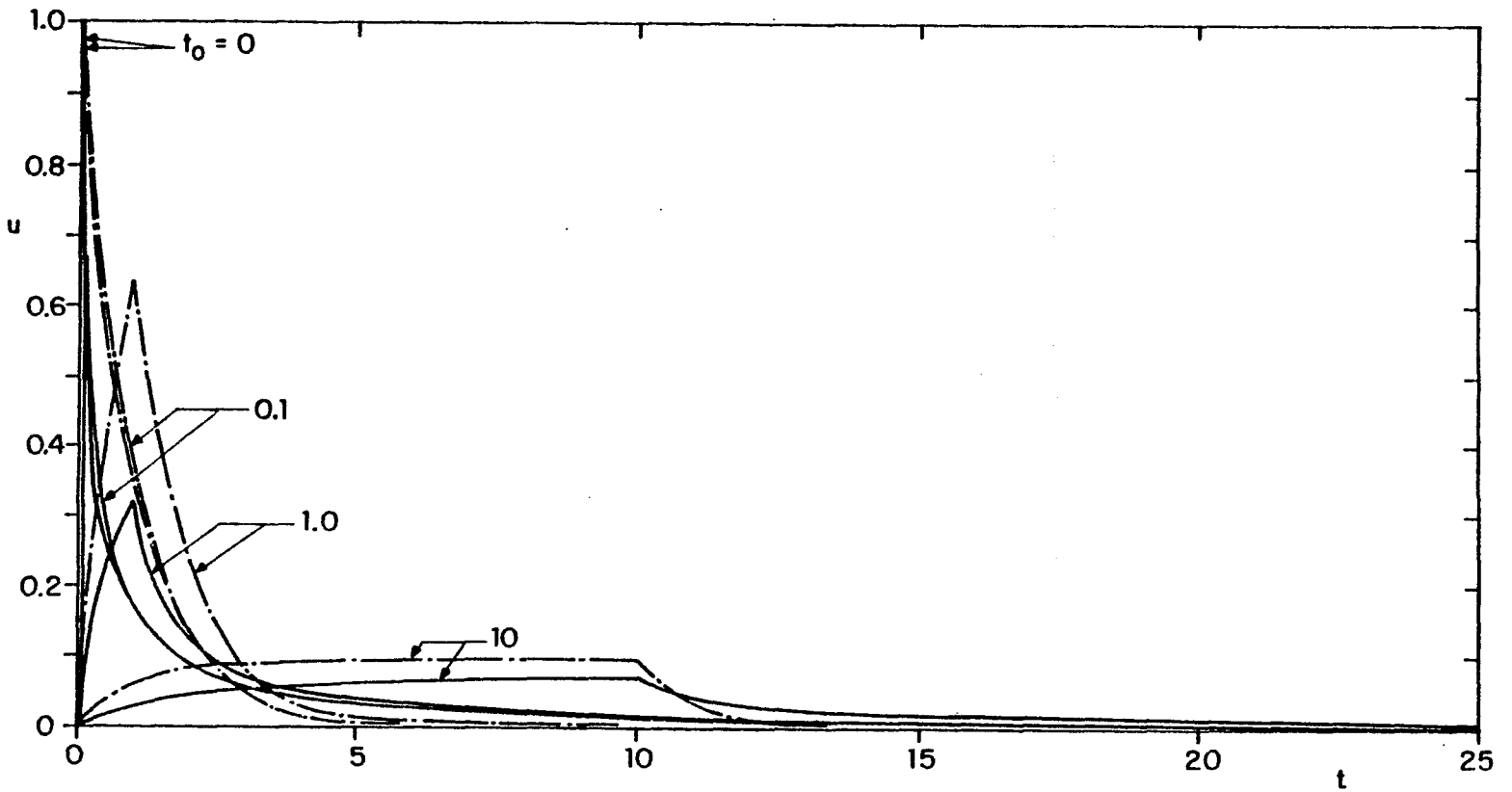

Figure I.4. Effect of duration, t_0, of a unit impulse on the velocity history of a sphere; —— constant force [Eqs. (I.15a) and (I.15b)], -•-•- constant force with $\tilde{F}_B = 0$ [Eqs. (I.16a) and (I.16b)].

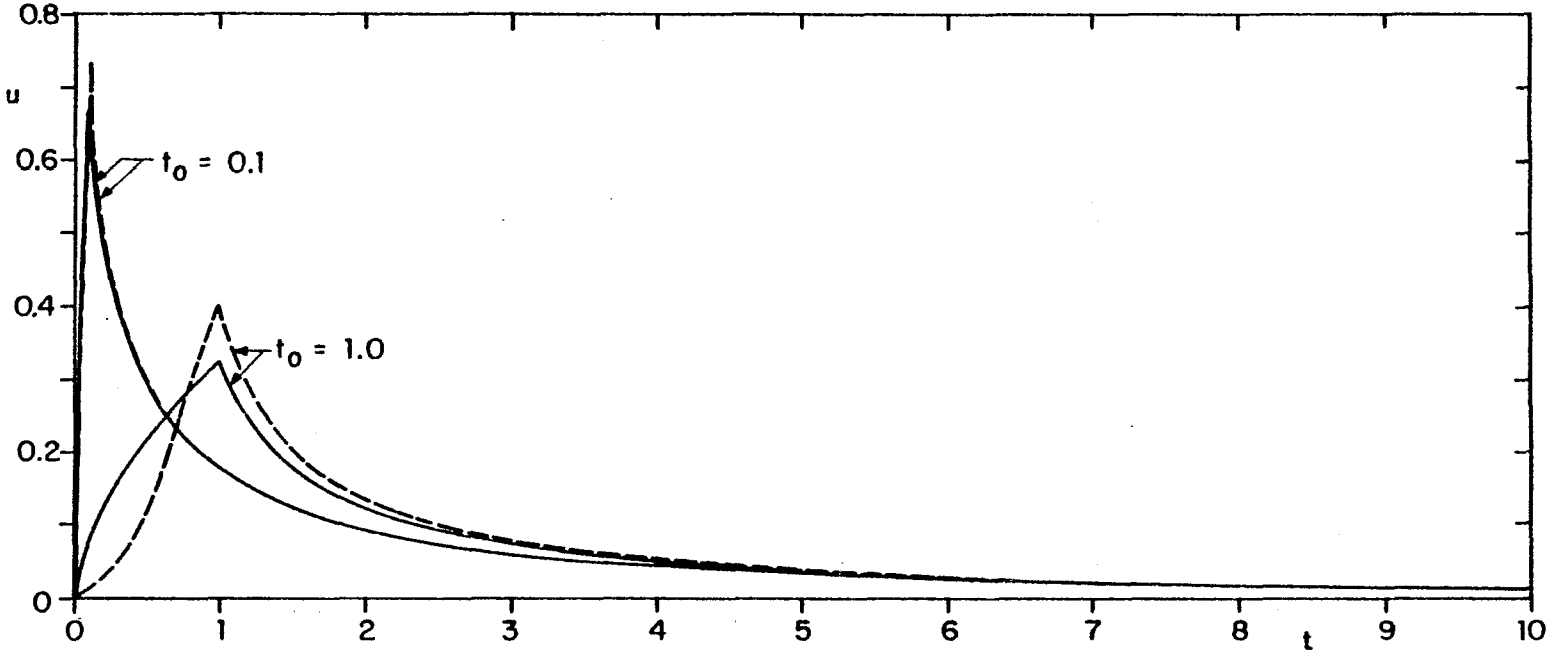

Figure I.5. Effect of duration, t_0, and waveform of a unit impulse on the velocity history of a sphere; ——— constant force [Eqs. (I.15a) and (I.15b)], ----- linear force [Eqs. (I.21a) and (I.21b)].

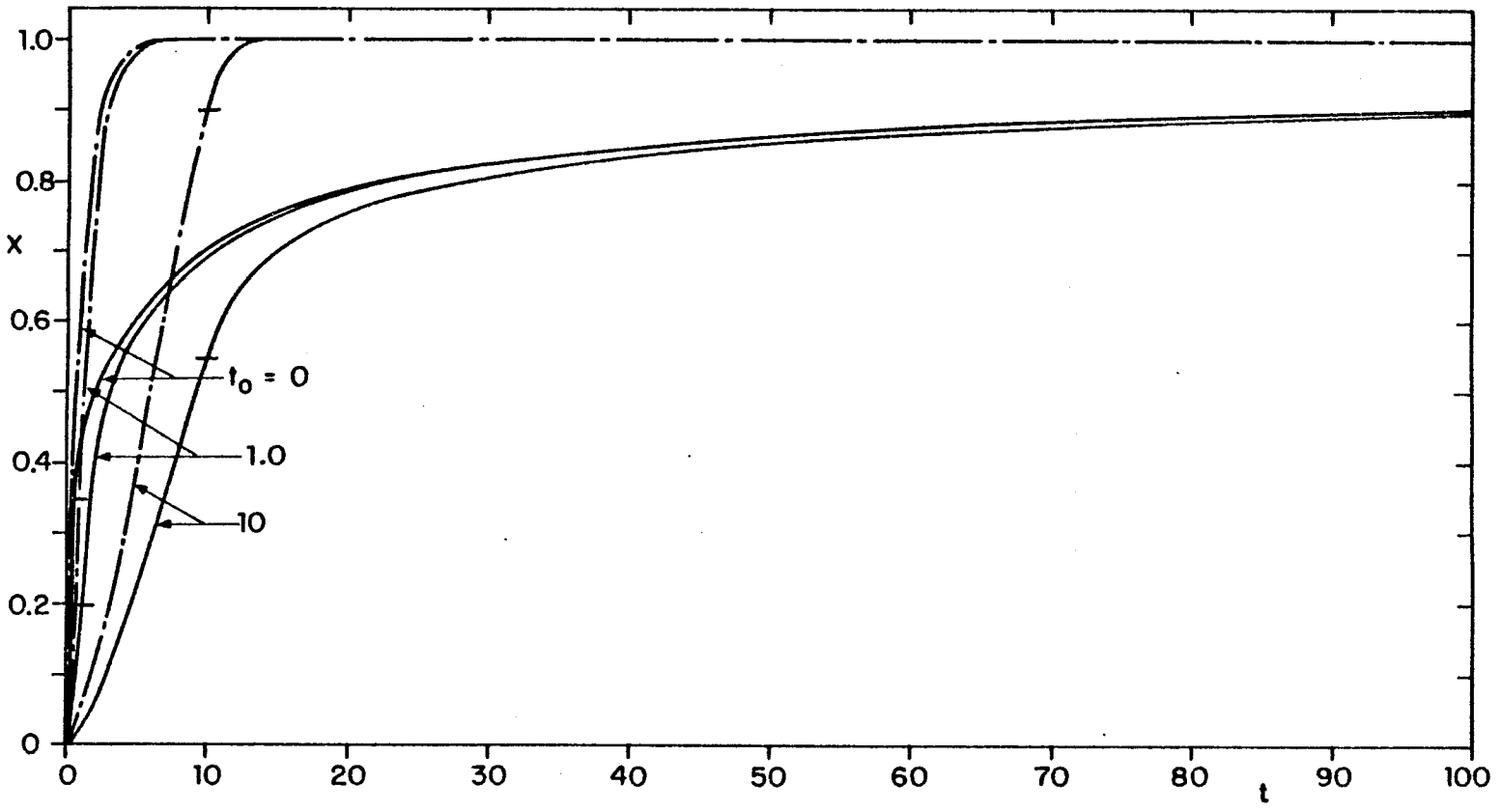

Figure I.6. Effect of duration, t_0, of a unit impulse on distance traveled by a sphere; —— constant force [from Eq. (I.15)], -•-•- constant force with $F_B = 0$ [from Eq. (I.16)]. Horizontal dash indicates beginning of relaxation phase.

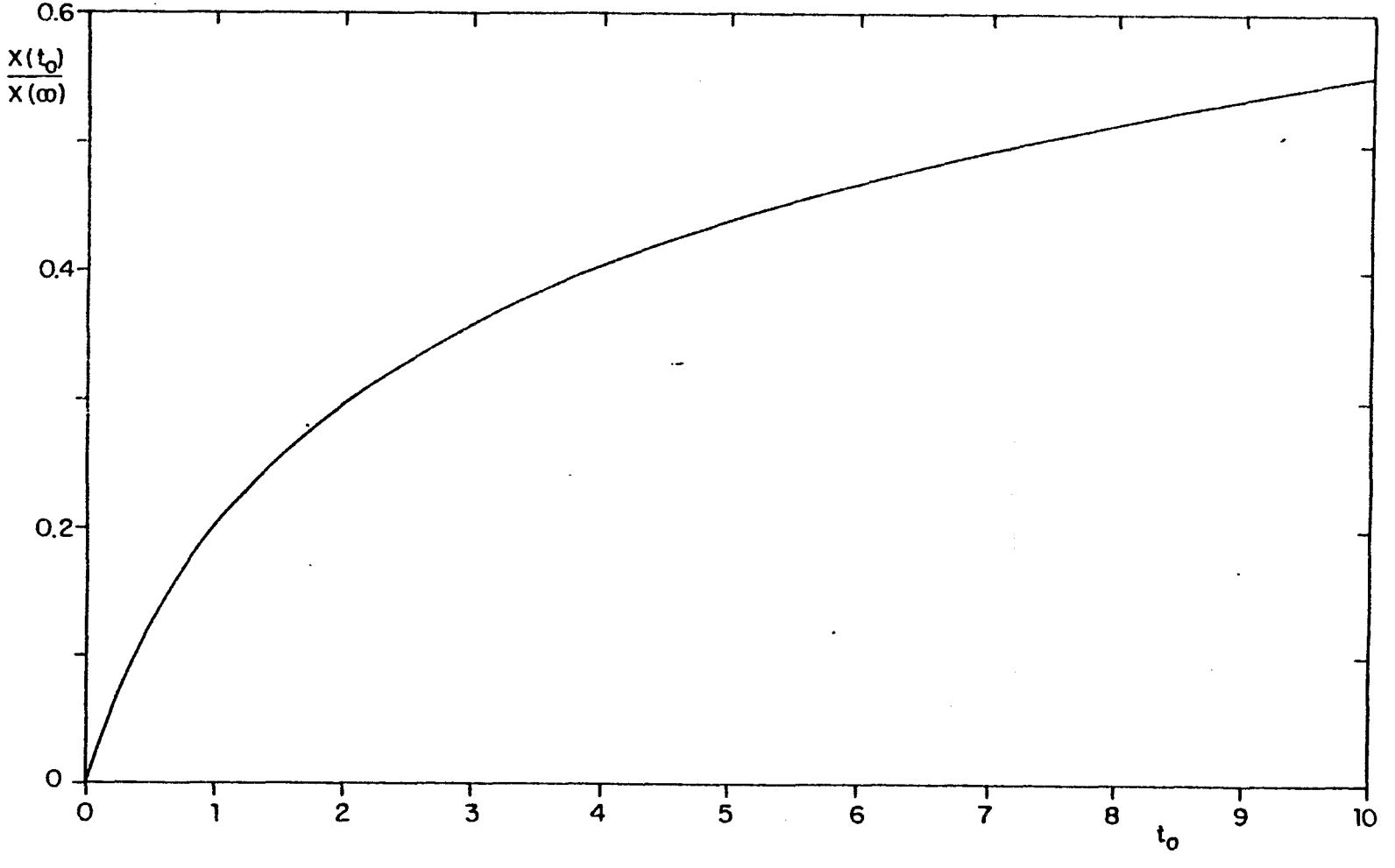

Figure I.7. Fraction of total distance traveled during duration, t_0, of a unit impulse by a sphere subject to a constant force [from Eq. (I.15)].

CHAPTER II

TIME DEPENDENT THEORY FOR VESICULAR TRANSPORT ACROSS VASCULAR ENDOTHELIUM

II-1. INTRODUCTION

A detailed description of the stages in the vesicular transport process outlined in the physiological background to this thesis is elaborated on in the first part of this chapter. A crude analysis is then offered for the mechanism of vesicle detachment and a time dependent labelling theory is subsequently presented and compared to existing experimental data.

Vesicles, when unimpeded by cytoplasmic structure, undergo a diffusional migration across cells which is strongly influenced by a hydrodynamic and molecular force interaction with the plasmalemma membranes of endothelial cells. In contrast to vesicles capable of endocytosis or exocytosis, which must be continuously created, and require metabolic energy and have a preferred direction of transport, plasmalemma vesicles are believed to be constant in population (at least on the time scale of laboratory experiments), derive their energy from thermal motions and be transported equally in both directions between the luminal and abluminal fronts (a net flux in one direction would cause a depletion in total vesicle population). The passive nature of the transport is supported by experiments with metabolic poisons (Newman and Zilversmit, 1966) and temperature dependent uptake (Siflinger, Caro and Parker, 1975). The conservation of the vesicle population results from the fact that the vesicle does not disappear in attaching to the plasmalemma but forms a quasi-stable attachment stalk as shown

in sketch (d) of Fig. II.1. An attached vesicle is subsequently released by the dissolution of the vesicle neck and the resealing of the vesicle and plasmalemma membranes.

The processes of vesicle attachment to and detachment from the plasmalemma are not symmetric. The sequence of events leading to vesicle attachment, as deduced from the electron micrographs of Palade and Bruns (1968), is schematically shown in Fig. II.1. When the vesicle approaches to within distances of 200 Å or less from the plasmalemma an attractive interaction is initiated which causes the plasma membrane to deform as shown in sketch (b). This long range attractive force is conjectured in Weinbaum and Caro (1976) to be electrodynamic in origin since the distances involved are typical of van der Waals force interactions in carefully controlled non-biological experiments (Israelachvili and Tabor, 1972). High magnification electron micrographs (see Fig. 19 Palade and Bruns, 1968) show that molecular level attractive forces are capable of narrowing the fluid gap to distances of 10 Å or less as depicted in sketch (c). This observation strongly suggests that the electric double layer forces between the exterior surface of the vesicle and the interior surface of the plasmalemma are much weaker than between the exterior surfaces of cell membranes. The negative surface charge on the exterior surfaces of cell membranes is believed to provide the repulsive energy that determines the much larger 20-150 Å equilibrium spacing typical of the intercellular junctions

observed between adjacent cells (Simionescu, Simionescu and Palade, 1975) and described theoretically in Weinbaum (1979). A general theory of electric double layers applied to biological membranes is presented in Parsegian (1973). As emphasized in a recent review article by Lodish and Rothman (1979), the exterior surface of a vesicle becomes the interior surface of a plasmalemma when attached and, therefore, has little negative charge since the sugar acid side chains are associated primarily with integral proteins inserted in the exterior leaflet of the membrane bilayer. The adhered configuration (c) is not stable at the molecular level and rapidly changes into the attached configuration (d), which is an integral part of the 75 Å molecular phospholipid bilayer structure of the plasmalemma membrane. Ultrastructural studies suggest that the transition from sketch (c) to (d) is accompanied by a viscoelastic flow of membrane material creating a transitory remnant which is thickest at the center of the newly formed vesicle stalk. This remnant appears to be short lived compared with the average residence time t_a of the vesicle in the attached state. In Weinbaum (1979) it is proposed that the open, attached vesicle shape is maintained by a ring-like force field of electrodynamic origin generated by intramembranous proteins that are observed in freeze-cleaved preparations of broken vesicle necks (see Fig. 16 Simionescu, Simionescu and Palade, 1974).

The detailed mechanics of vesicle detachment from the plasmalemma is not known, although as stated previously the process seems to be passive and derive its energy from the thermal motion of the surrounding water molecules. The vesicle attachment stalk appears to undergo a membrane flow or dissolution process that takes the vesicle from configuration (d) to its free resealed spherical shape without passing through the double membrane configuration (c). If the vesicle is in thermodynamic equilibrium with its surroundings, the mean thermal velocity of the vesicle at 37°C, which has a density equal to that of water, is roughly 30 cm/sec. When this result is substituted in equations (I.6) and (I.12) along with the physical parameters of the problem it is possible to estimate that the fluctuations due to individual collisions are of the order 0.05 nm or less. The feasibility of the propagation of a larger amplitude elastic wave through the vesicle neck is examined in section II-2a.

A convenient way to study the vesicular transport process is to supply and monitor a uniform source of labelled macromolecules at the luminal surface (see Fig. II.2). Tomlin (1969) estimates that the loading of macromolecules in the absence of molecular sieving occurs in the order of 10^{-2} sec, a time which is at least two orders of magnitude shorter than the mean attachment time t_a. Molecular sieving effects have been observed for larger molecules, e.g. ferritin, molecular diameter 11-12 nm (Casley-Smith and Chin, 1971; Clough and Michel, 1978). As time progresses the

labelled vesicles diffuse to the abluminal surface eventually establishing a steady state concentration profile. While there have been several time dependent vesicle labelling studies performed to date, the only investigation that attempts to quantitatively report this transient sequence of events is Casley-Smith and Chin (1971). These authors measured the proportions of labelled cytoplasmic vesicles at increasing distances across mouse heart endothelium and diaphragmatic mesothelium using the tracers ferritin, horseradish peroxidase, and sodium ferrocyanide. The cells were incubated in Hank's solution containing the tracer for periods of 2 sec up to 30 min at 37°C.

While there are numerous physical processes involved in the overall vesicular transport function, including hydrodynamic and electrodynamic interactions, chemical and electric double layer effects and membrane elastic and viscoelastic deformations, the two processes that can be separated out because they occur on longer length scales than the others are the hydrodynamic and long range electrodynamic interactions between the vesicle and the boundary plasmalemmas. Hydrodynamic effects are shown in Weinbaum and Caro (1976) and the present study to be important throughout the cell interior since the average transendothelial diffusion distance, which varies from 1.5 to 3.5 μm for capillary endothelium and 3 to 5 μm for arterial endothelium, is only 2 to 7 times the vesicle diameter. Van der Waals forces, although they extend only several

hundred Å from each plasmalemma, are significant since they occur in a range where the spatial variation of the hydrodynamic resistance and hence the diffusion coefficient is rapidly changing. The effective van der Waals interaction length will thus be shown in section II-3b to have an important effect on the steady state permeability. All the other factors, which are primarily associated with the vesicle attachment/detachment process, shall not be distinguished but lumped into single reaction rate constants describing the formation/dissolution of the vesicle attachment stalks.

In the past decade a variety of theoretical models have been introduced to quantitatively study both steady state vesicular transport (Tomlin, 1969; Shea, Karnovsky and Bossert, 1969; Green and Casley-Smith, 1972; Shea and Bossert, 1973; Weinbaum and Caro, 1976) and time dependent labelling experiments (Rubin, 1977). The earliest of the steady state models were based on one-dimensional continuum diffusion theory (Tomlin, 1969) or random walk computer simulation experiments (Shea, Karnovsky and Bossert, 1969) in which the interaction of the vesicle with the boundary plasmalemmas was neglected entirely and a constant diffusion coefficient assumed based on infinite domain Stokes-Einstein diffusion theory. It was soon realized because of the poor agreement of the predicted steady state concentration profiles and the available experimental data that interactions near the plasmalemma played a vital role in the transport

process. To remedy this shortcoming Green and Casley-Smith (1972) and Shea and Bossert (1973) proposed an ad hoc phenomenological approach in which the wall was modeled as an imperfectly absorbing barrier with an elastic reflection coefficient. The value of the coefficient was empirically determined so as to provide a reasonable curve fit with experimental data.

The first dynamic model of the steady state vesicular transport process, which attempts to consider in an approximate manner the hydrodynamic and molecular force interaction between the vesicle and the plasmalemma, is presented in Weinbaum and Caro (1976). In this model a theoretical expression is derived for the spatial variation of the diffusion coefficient, which considers the increased hydrodynamic resistance of the vesicle as it approaches the plasma membranes on each side of the cell, and for the van der Waals electrodynamic attractive force between the vesicle and the boundary plasmalemmas. This more complete model still neglects the chemical, elastic, and viscoelastic energy involved in the formation and dissolution of the vesicle attachment stalks. These latter processes, the formation and dissolution of the vesicle neck, are treated as a free energy barrier within the framework of absolute reaction rate theory in Rubin (1977). Rubin also shows how the vesicle attachment/detachment processes can be combined with the diffusion of free vesicles in the cell interior to define a steady state permeability coefficient

for the entire vesicle transport process.

Rubin (1977), in addition, presents a simplified time dependent mathematical model to theoretically predict the initial stages of time dependent vesicle labelling experiments. The vesicle motion in the cell interior is described by a one-dimensional, unsteady diffusion with a constant diffusion coefficient while the vesicle attachment/detachment process at the luminal surface is described by the same reaction rate theory as in the steady state model. Solutions are presented for the case where the abluminal plasma membrane is assumed to be at infinity and the processes of vesicle attachment/detachment are incorrectly considered to be a mirror image sequence of events. These solutions are valid only for very short times, because of the neglect of the second plasma membrane, and can not be used to describe the approach to steady state labelling.

It is the purpose of this chapter to develop a time dependent vesicle labelling theory valid for all time which considers the spatial dependence of the diffusion coefficient and the convective velocity induced by van der Waals attractive forces near the plasma membranes by extending the basic model of Weinbaum and Caro (1976) to time dependent vesicle diffusion. As in the steady state theory the complication introduced by the shift between non-retarded and retarded electrodynamic forces, molecular interference effects and electric double layer forces will all be neglected. One factor which is considered in chapter III is the increased

hydrodynamic resistance due to steric crowding of attached vesicles (see for example, Fig. 2 of Simionescu, Simionescu and Palade, 1974) as a vesicle approaches a plasmalemma membrane. This chapter will also show how Rubin's one-dimensional model for the steady state permeability can be generalized to include an arbitrary spatial variation of the diffusion coefficient for a variable hydrodynamic resistance law in the cell interior.

The next section is devoted to a theoretical formulation of the overall problem. Section II-3 describes the solution procedure while section II-4 presents the numerical results. These results are discussed in section II-5 and compared with the time dependent tracer data of Casley-Smith and Chin (1971).

II-2. DYNAMIC MODELS OF THE VESICLE MOTION

This section is devoted to a theoretical formulation of the overall transendothelial vesicle motion. This motion is characterized by five different length scales (see Fig. II.2): a short length ϵ_0, representative of London-van der Waals electrodynamic forces, a hydrodynamic interaction length characteristic of the vesicle-cell membrane interaction, the vesicle radius a and release distance y and the transendothelial diffusion distance ℓ. Section II-2a discusses the mechanics of vesicle detachment, section II-2b examines the near field approach of the vesicles to each plasmalemma, and section II-2c studies the spatially varying long range hydrodynamic interaction with both plasmalemmal boundaries.

II-2a. Formation/Dissolution of Vesicle Attachment Stalk

As discussed in section II-1 there are several complex elastic, chemical and viscoelastic processes involved in the formation or dissolution of the vesicle attachment stalk. Since these processes can not be distinguished at present, all these effects will be lumped together into single reaction rate constants describing either the overall formation or dissolution process. Following the approach presented in Rubin (1977) the rupture or formation of the vesicle neck attachment membrane can be thought of as a free energy barrier. If $\Delta G^d_{\pm i}$ is the activation energy associated with the formation or rupture of the membrane diaphragm of an attached vesicle where $\pm$ describe the direction with

respect to the x-axis, then a rate constant $k^{d}_{\pm i}$ can be expressed which describes the velocity of the reaction as:

$$K^{d}_{\pm i} = \lambda_i^{o,d} K^{o,d}_{\pm i}$$

$$= \lambda_i^{o,d} \chi^{d}_{\pm i} (\kappa T/h) \exp(-\Delta G^{d}_{\pm i}/RT), \qquad \text{(II.1)}$$

Here $\lambda_i^{o,d}$ is the length of the reaction zone traversed between initial and final state configurations; $k^{o,d}_{\pm i}$ is a reaction rate constant according to absolute reaction rate theory (Glasstone, Laidler and Eyring, 1941) and is defined in terms of the transmission coefficient $\chi^{d}_{\pm i}$, the Boltzmann constant k, the Planck constant h, the temperature T, the free energy of activation $\Delta G^{d}_{\pm i}$ and the molar gas constant R and i indicates the region where the reaction is taking place.

Additional insight into a possible mechanism for the rupture of the vesicle attachment stalk can be obtained from the following crude order of magnitude analysis. If the energy for the vesicle release comes from thermal motions, as is currently believed, then this energy can be used to elastically deform the vesicle membrane. Any such deformation is transitory and must propagate as an elastic wave through the vesicle neck. The question of interest is whether the wavelength of a thermally produced wave of this nature is of the same order as the length of the vesicle attachment stalk. If the wavelength were large

compared to this dimension, say 10^4 or 10^6 Å, then a large amplitude deformation could not be produced in the vesicle neck membrane and the proposed elastic wave rupture mechanism would not be feasible.

Suppose that the nearly spherical wall of a vesicle of radius a is deforming under Brownian motion. If one neglects the elastic restoring forces of the membrane, the probability that any portion of the vesicle membrane will be located in a spherical shell of thickness dr at a distance r-a from its initial position r=a at t=0 at time t is:

$$w(r-a,t) = \frac{(r-a)^2 e^{-(r-a)^2/4D_o t}}{2\sqrt{\pi}\,(D_o t)^{3/2}}\,dr, \qquad \text{(II.2)}$$

where the diffusion coefficient D_o is approximated by the Stokes-Einstein relation for a spherical particle in an infinite medium, $D_o = kT/6\pi\mu_o a$. The root mean square displacement of the boundary from its initial position is given by:

$$\overline{(r-a)^2} = \int_o^\infty (r-a)^2 w(r-a,t) = 6 D_o t \qquad \text{(II.3)}$$

From equations (II.2) and (II.3) the time t required for a portion of the boundary to be displaced the root mean square distance $\overline{(r-a)^2}$ is:

$$t = \frac{\pi \mu_o a \overline{(r-a)^2}}{kT} \qquad \text{(II.4)}$$

Assume now that a deformation in the body of an attached vesicle propagates into the neck region. Considering geometric factors and neglecting viscous damping, a 3.5-5 nm displacement in the neck would be produced by a roughly 1 nm distortion in the main body of the vesicle. The speed of propagation of an elastic wave in a flexible cylindrical tube of radius R typical of the vesicle neck which contains a viscous fluid of viscosity μ_o is given in Lightfoot (1974) p. 120 as:

$$c' = \frac{R}{2}\sqrt{\frac{Eh'\omega}{2R\mu_o}} \qquad \text{(II.5)}$$

where ω is the wave frequency, h' the membrane thickness, and E Young's modulus. Equation (II.5) is valid in the limit where the decay time of the fluid motion is small compared to the driving period $1/\omega$. If the time t in equation (II.4) is of order $1/\omega$, the wavelength of the wave in the neck region is given by:

$$\lambda' \sim c't = \frac{R}{2}\sqrt{\frac{Eh'}{2R\mu_o t}} \qquad \text{(II.6)}$$

Equations (II.5) and (II.6) have been evaluated using R = 10 nm (vesicle neck radius), $\overline{(r-a)^2} = 1\text{nm}^2$, h' = 7.5 nm (membrane bilayer thickness), μ_o = 2 centipoise (this is based on the water inside the vesicle not the intracellular viscosity) and a value of E characteristic of the red cell membrane. One finds $c' \sim 0.4$ cm/sec and that $\lambda' \sim 20$ nm.

The close numerical agreement between the predicted wavelength based on this crude theory and the vesicle neck length is fortuitous. However, the qualitative agreement supports the hypothesis that the mechanism of vesicle detachment derives from thermally induced fluctuations of the vesicle neck membrane.

II-2b. The van der Waals Force Layers

Following the general approach for steady state vesicle diffusion proposed in Weinbaum and Caro (1976), it is desired to develop separate but related analyses for the vesicle motion in the narrow regions $0 < x < \epsilon$ and $1-\epsilon < x < 1$* near each plasmalemma where molecular level electrodynamic forces are important and in the cell interior where these effects can be neglected but the hydrodynamic interaction with both plasmalemma boundaries is significant. As in the steady state model an effective dimensional cut-off distance for the van der Waals forces ϵ_0 is defined and the near field solutions adjacent to each plasmalemma are matched asymptotically for $x/\epsilon_0 >> 1$ with the time dependent solutions for the vesicle diffusion in the interior of the cell.

The conservation equation for the vesicle number density c on each side of the plane of release x = y

* For convenience the x coordinate will henceforth be shifted to the center of the diffusing vesicle and the origin shifted a vesicle radius inward from the luminal surface in Fig. II.2. The total distance available for diffusion ℓ is thus the width of the cell minus 2a. If all distances are scaled relative to ℓ, then the dimensionless cut-off distance for the van der Waals forces $\epsilon = \epsilon_0/\ell$.

can be described by a continuum equation of the form (all quantities in dimensional form):

$$\frac{\partial c}{\partial t} + \frac{\partial c u_{vw}}{\partial x} = \frac{\partial}{\partial x}\left(D(x)\frac{\partial c}{\partial x}\right) \quad \begin{matrix} 0<x<y \\ y<x<\ell, \end{matrix} \qquad \text{(II.7)}$$

where u_{vw} can be thought of as a convective velocity for the vesicles created by the macroscopic London-van der Waals force and D is a spatially varying diffusion coefficient which takes account of the hydrodynamic interactions with the boundaries. A similar set of equations can also be written for the vesicles released at the plane $x = \ell - y$. The mean free path of of an individual thermal excursion x_e, as indicated in section II-1, has been estimated as 0.5 Å or less. Since the characteristic near field distance ϵ_0 is of order 10 Å or larger, $x_e/\epsilon_0 << 1$ and the continuum hypothesis is justified.

The expression for D(x) is obtained by introducing an effective viscosity $\mu(x) = \lambda(x)\mu_0$ into the Stokes-Einstein relation for the diffusion coefficient where μ_0 is the actual fluid viscosity and λ is a hydrodynamic interaction parameter describing the variation in fluid resistance for the perpendicular motion of a spherical particle between two parallel walls. Thus:

$$D(x) = D_0/\lambda(x), \qquad \text{(II.8)}$$

where D_0 is the vesicle diffusion coefficient in an

infinite medium.

An exact solution for λ for a spherical particle of arbitrary size and position between two planar walls has recently been obtained by Ganatos, Weinbaum and Pfeffer (1979). This solution was determined by the superposition of disturbances generated by the particle and the confining walls. The particle disturbances were represented as an infinite series with each term containing an unknown coefficient while the wall disturbances were expressed in the form of a Fourier-Bessel integral containing unknown functions. These unknown functions were determined by analytic inversion of the disturbances produced by the sphere and felt on the confining walls so that the no-slip boundary conditions would be satisfied exactly along the walls. The coefficients introduced by the particle were then determined by a collocation technique in which the infinte series was truncated and the no-slip boundary conditions applied at discrete points on the surface of the spherical particle. Prior to this an exact solution was only available for the motion near a single wall (Cox and Brenner, 1968) and an approximate solution available for the motion between two parallel boundaries for the case $a/\ell \ll 1$ (Ho and Leal, 1974).

A close approximation to the exact solution presented in Ganatos et al can be written in the form:

$$\lambda = \beta + \frac{\theta a}{x} + \frac{\theta a}{1-x}, \qquad \text{(II.9)}$$

where the constants θ and β are chosen to provide a least squares fit with the exact results. θ is a correction to the Taylor lubricating film resistance at each plasmalemma and β is a correction for the combined interaction of the walls. Table II.1 shows a comparison between the approximate expression (II.9) and the exact solution for a representative value of a/ℓ. Equation (II.9) provides a small improvement over the expression for λ used previously in Weinbaum and Caro (1976) for the particular value of ℓ used in this table, but a more significant correction as ℓ decreases.

In the region of electrodynamic interaction $x = O(\epsilon_0)$ near the luminal plasmalemma $\theta\, a/x >> 1$ and $\lambda(x)$ from (II.9) is approximately equal to $\theta\, a/x$, thus from equation (II.8) $D(x) \approx D_0 x/a\theta$. Substituting this expression in (II.7) and scaling the coordinate x relative to ϵ_0, the characteristic near field dimension, one obtains:

$$\epsilon_0 \frac{\partial c}{\partial t} + \frac{\partial c u_{vw}}{\partial x^*} = \frac{D_0}{\theta a} \frac{\partial}{\partial x^*}\left(x^* \frac{\partial c}{\partial x^*}\right) , \qquad \text{(II.10)}$$

where $x^* = x/\epsilon_0$.

The following scaled variables are introduced into equation (II.10):

$$c^* = \frac{c D_0}{\phi \ell} , \quad t^* = \frac{t D_0}{\ell^2} , \quad u_{vw}^* = \frac{u_{vw} a}{D_0} , \qquad \text{(II.11)}$$

where ϕ is the vesicle release rate per unit area of luminal surface and D_0/a is a reference diffusion velocity. The dimensionless form of equation (II.10) is:

$$\frac{a\epsilon_0}{\ell^2}\frac{\partial c^*}{\partial t^*} + \frac{\partial c^* u^*_{vw}}{\partial x^*} = \frac{1}{\theta}\frac{\partial}{\partial x^*}\left(x^*\frac{\partial c^*}{\partial x^*}\right). \qquad \text{(II.12)}$$

Since $\epsilon_0 a/\ell^2$ is of $O(10^{-2})$ or smaller, one concludes that the unsteady term in equation (II.12) is small compared to the other terms present in the van der Waals layer. The time required to achieve a quasi-steady near field solution is of order $\epsilon_0 a/D_0$ and thus is of $O(\epsilon_0 a/\ell^2)$ shorter than the characteristic diffusion time for the cell interior. The narrow van der Waals force layers near each plasmalemma therefore develop in a quasi-steady manner with a nearly steady state concentration profile that is slowly changing in response to events that occur in the cell interior.

The quasi-steady state solution to equation (II.12) with appropriate changes in nomenclature, is found in Weinbaum and Caro (1976):

$$\frac{c^* \phi \ell}{\theta a A(t^*)} = \frac{1}{3}\ln\left[1 + (\kappa/\epsilon_0)^3\right], \qquad \text{(II.13)}$$

where the function $A(t^*)$ is slowly varying on the near field time scale $\epsilon_0 a/D_0$. This solution is based on a simplified description of the van der Waals force interaction in which non-retarded forces are summed over an

undeformed spherical vesicle and planar plasmalemma for an arbitrary fluid gap x.

The function $A(t^*)$ is unknown, but will be determined by matching the behavior of the near field solution for $x/\epsilon_0 \gg 1$ with the large scale solution for the vesicle density distribution in the interior of the cell. As shown in Fig. 6 of Weinbaum and Caro the effective van der Waals force layer thickness ϵ_0 is defined as the distance from the plasmalemma at which the free vesicle concentration would vanish for the solution in the cell interior if electrodynamic forces were not present. The dimensionless distance $\epsilon = \epsilon_0/\ell$ plays the same role as a displacement thickness in fluid boundary-layer theory.

II-2c. Vesicle Diffusion in the Cell Interior

In the interior of the cell the convective velocity term in equation (II.7) describing the van der Waals force interaction with the plasmalemma boundaries vanishes. In this region x is scaled relative to the transendothelial diffusion distance ℓ and t scaled relative to the characteristic diffusion time ℓ^2/D_0. The dimensionless vesicle conservation equation for vesicles released at the luminal surface is (asterisk dropped):

$$\frac{\partial c}{\partial t} = \frac{\partial}{\partial x}\left(\frac{1}{\lambda(x)}\frac{\partial c}{\partial x}\right) \qquad \begin{matrix} \epsilon \le x \le y^- , \\ y^+ \le x \le 1-\epsilon . \end{matrix} \qquad \text{(II.14)}$$

The region of validity of (II.14) excludes the vesicle

release point x = y and the small regions $0 \leq x \leq \epsilon$ and $1-\epsilon \leq x \leq 1$ near each plasmalemma. ϵ is defined by the apparent-boundary concept or effective London-van der Waals displacement distance described in section II-2b. In accord with this definition it is required that at $x = \epsilon$ and $x = 1-\epsilon$:

$$c(\epsilon, t) = 0 \qquad \text{(II.15a)}$$

$$c(1-\epsilon, t) = 0 . \qquad \text{(II.15b)}$$

Initially, there are no labelled vesicles so that:

$$c(x,0) = 0 . \qquad \text{(II.16)}$$

At x = y, the average intrusion distance for vesicles released from the luminal membrane, the concentration of free vesicles is continuous:

$$c(y^-,t) = c(y^+,t) , \qquad \text{(II.17)}$$

but there is a discontinuity in concentration gradient. In dimensionless form this discontinuity in flux is given by:

$$1 = \frac{1}{\lambda(y)} \left[\frac{\partial c(y^-,t)}{\partial x} - \frac{\partial c(y^+,t)}{\partial x} \right] . \qquad \text{(II.18)}$$

Equation (II.14) is also valid in the range $\epsilon \leq x < 1-y$ and $1-y < x \leq 1-\epsilon$ for vesicles released at the abluminal surface, where at x = 1-y equivalent matching conditions to (II.17) and (II.18) hold. Statistical studies performed by

Bruns and Palade (1968) and Casley-Smith (1969) for the number density profile of free vesicles in the cell interior and attached vesicles at each plasmalemma show that the vesicle transport is nearly symmetric.

II-3. SOLUTIONS FOR VESICLE CONCENTRATION, FLUX AND STEADY STATE PERMEABILITY

The boundary value problem defined by equations (II.14) through (II.18) for the vesicle diffusion in the multi-layered region $\epsilon \leq x < y$ and $y < x \leq 1-\epsilon$ is equivalent to that arising in one-dimensional unsteady heat transfer in more than a single slab. Whereas the steady state problem is straightforward, the unsteady problem has only been solved for the case of constant diffusivity. Even with the simplification of constant diffusivity the mathematical problem is difficult and has been solved only recently using newly developed normalization techniques. The difficulty stems from the fact that the matching conditions for the temperature (concentration) and its gradient are unknown functions of time at the interface between regions. A novel approximate integral solution technique is developed in section II-3a for treating the variable diffusivity problem. This approximate solution method is considerably less expensive than finite difference schemes. In section II-3b an expression will be derived for the steady state permeability of the cell layer in which the description of the attachment/detachment process described in section II-2a will be coupled to the solutions for the vesicle diffusion in the cell interior.

II-3a. Solution for Time Dependent Vesicle Diffusion

The conceptual formulation of the integral solution technique for solving the boundary and initial value problem

in the cell interior is schematically illustrated in Fig. II.3. One can consider two coupled boundary layers of thickness $\delta_1(t)$ and $\delta_2(t)$ spreading from the vesicle plane of release. There are three different time domains of solution. For $t \leq t_1$ both boundary layers diffuse until the one on the left reaches $x = \epsilon$ and $\delta_1(t_1) = y - \epsilon$. The boundary layer to the right of $x = y$, however, has not yet reached $x = 1 - \epsilon$. This marks the beginning of the second time domain $t_1 \leq t \leq t_2$. In this time domain the right boundary layer continues to grow towards $x = 1 - \epsilon$, while the left remains fixed at $x = \epsilon$, satisfying equation (II.15a), but with a time dependent concentration gradient at $x = \epsilon$. This behavior continues until the right boundary layer reaches $x = 1 - \epsilon$ and $\delta_2(t_2) = 1 - \epsilon - y$. In the third time domain $t_2 \leq t \leq t_\infty$ both boundary layers satisfy equation (II.15) at their ends $x = \epsilon$ and $x = 1 - \epsilon$, but their concentration gradients at these locations will vary until a steady state is asymptotically achieved.

Because the hydrodynamic resistance increases as a/x as the vesicles approach each membrane, the concentration profile in the steady state is logarithmic and cannot be described by a simple lower order polynomial in x. Thus, to achieve the proper asymptotic behavior the following transformation of coordinates is first introduced into equations (II.14) to (II.18):

$$d\varsigma = \lambda(x)\,dx. \qquad \text{(II.19)}$$

Equation (II.14) now becomes:

$$\frac{\partial c}{\partial t} = \lambda(x)\frac{\partial^2 c}{\partial \varphi^2}, \qquad \begin{matrix} \epsilon < x < y \\ y < x < 1-\epsilon, \end{matrix} \qquad \text{(II.20)}$$

where it is observed that in the steady state c is a linear function of φ. One is thus able to achieve the correct steady state solution by assuming a polynomial profile for c in the transformed φ coordinate. The concentration profiles on each side of the plane of release x = y are

$$c_1 = a_1 + a_2\varphi + a_3\varphi^2, \qquad x < y, \qquad \text{(II.21a)}$$

$$c_2 = a_4 + a_5\varphi + a_6\varphi^2, \qquad x > y. \qquad \text{(II.21b)}$$

The transformed boundary and matching conditions, equations (II.15), (II.17) and (II.18) are:

$$c(\varphi(\sigma_1),t) = 0 \qquad \text{(II.22a)}$$

$$c(\varphi(\sigma_2),t) = 0 \qquad \text{(II.22b)}$$

$$c(\varphi(y^-),t) = c(\varphi(y^+),t) \qquad \text{(II.23)}$$

$$1 = \frac{\partial c(\varphi(y^-),t)}{\partial \varphi} - \frac{\partial c(\varphi(y^+),t)}{\partial \varphi}, \qquad \text{(II.24)}$$

where the subscripts 1 and 2 refer to conditions on the left and right of the plane of release (x = y) respectively and σ_1 and σ_2 are the distances from the origin of each boundary layer edge:

$$\sigma_1 = y - \delta_1 \qquad \text{(II.25a)}$$

$$\sigma_2 = \delta_2 + y. \qquad \text{(II.25b)}$$

Once the boundary layers have reached the effective boundaries of the cell $x = \epsilon$ and $x = 1-\epsilon$ at times t_1 and t_2 respectively, δ_1 and δ_2 no longer change but the absolute

value of the concentration gradient at each edge increases until its steady state value is achieved. The transformed concentration gradients, which are denoted by:

$$\alpha_1(t) = \frac{\partial c(\mathcal{Y}(\epsilon), t)}{\partial \mathcal{Y}}, \quad t > t_1 \tag{II.26a}$$

$$\alpha_2(t) = \frac{\partial c(\mathcal{Y}(1-\epsilon), t)}{\partial \mathcal{Y}}, \quad t > t_2, \tag{II.26b}$$

thus replace δ_1 and δ_2 as the unknown parameters in the integral equation formulation.

When $t < t_1$ or t_2, as the case may be, and one or both of the boundary layers have not reached their respective cell boundaries, the edge conditions (II.26a,b) are replaced by the requirement that the concentration gradient vanish at the boundary layer edge. Thus, at $x = \sigma_1$ and σ_2:

$$\frac{\partial c(\mathcal{Y}(\sigma_1), t)}{\partial \mathcal{Y}} = 0, \quad t < t_1 \tag{II.27a}$$

$$\frac{\partial c(\mathcal{Y}(\sigma_2), t)}{\partial \mathcal{Y}} = 0, \quad t < t_2. \tag{II.27b}$$

The relation between the transformed distance coordinate $\mathcal{Y}$ and x is obtained by integrating equation (II.19) from $\mathcal{Y} = 0$ at $x = \epsilon$ to $\mathcal{Y} = \mathcal{Y}$ at $x = x$. The result is:

$$\mathcal{Y}(x) = \beta(x-\epsilon) + \theta a \ln\left[\frac{x(1-\epsilon)}{(1-x)\epsilon}\right] \tag{II.28}$$

The above choice of origin of the $\mathcal{S}$ coordinate significantly simplifies the solutions for both the transient vesicle flux and the steady state concentration profile.

The six unknown coefficients a_i, $i = 1,\ldots 6$, in equations (II.21a,b) are determined by the boundary and matching conditions (II.22) through (II.27). The resulting concentration profiles in the three time domains are:

$$0 \le t \le t_1: \quad c_1 = c(\mathcal{S}(Y),t)\left[\frac{\mathcal{S}(\sigma_1)-\mathcal{S}(X)}{\mathcal{S}(\sigma_1)-\mathcal{S}(Y)}\right]^2 \qquad \text{(II.29a)}$$

$$c_2 = c(\mathcal{S}(Y),t)\left[\frac{\mathcal{S}(\sigma_2)-\mathcal{S}(X)}{\mathcal{S}(\sigma_2)-\mathcal{S}(Y)}\right]^2 \qquad \text{(II.29b)}$$

where

$$c(\mathcal{S}(Y),t) = \left[\frac{(\mathcal{S}(Y)-\mathcal{S}(\sigma_1))(\mathcal{S}(Y)-\mathcal{S}(\sigma_2))}{2(\mathcal{S}(\sigma_1)-\mathcal{S}(\sigma_2))}\right] \qquad \text{(II.29c)}$$

$$t_1 \le t \le t_2: \quad c_1 = \alpha_1(t)\,\mathcal{S}(X) + \left[\frac{c(\mathcal{S}(Y),t)-\alpha_1(t)\mathcal{S}(Y)}{\mathcal{S}^2(Y)}\right]\mathcal{S}^2(X) \qquad \text{(II.30a)}$$

$$c_2 = c(\mathcal{S}(Y),t)\left[\frac{\mathcal{S}(\sigma_2)-\mathcal{S}(X)}{\mathcal{S}(\sigma_2)-\mathcal{S}(Y)}\right]^2 \qquad \text{(II.30b)}$$

where

$$c(\mathcal{S}(Y),t) = \left(\frac{1+\alpha_1(t)}{2}\right)\left[(\mathcal{S}(\sigma_2)-\mathcal{S}(Y))\,\mathcal{S}(Y)/\mathcal{S}(\sigma_2)\right] \qquad \text{(II.30c)}$$

$$t_2 \leq t \leq t_\infty: \quad c_1 = \alpha_1(t)\,\varphi(x) + \left[\frac{c(\varphi(y),t) - \alpha_1(t)\,\varphi(y)}{\varphi^2(y)}\right]\varphi^2(x) \tag{II.31a}$$

$$c_2 = \alpha_2(t)\left[\varphi(x) - \varphi(1-\epsilon)\right] + (\varphi(x) - \varphi(1-\epsilon))^2\left[\frac{c(\varphi(y),t) - \alpha_2(t)(\varphi(y) - \varphi(1-\epsilon))}{(\varphi(1-\epsilon) - \varphi(y))^2}\right] \tag{II.31b}$$

where

$$c(\varphi(y),t) = \frac{(1 + \alpha_1(t) - \alpha_2(t))\varphi(y)(\varphi(1-\epsilon) - \varphi(y))}{2\,\varphi(1-\epsilon)}. \tag{II.31c}$$

Equation (II.20) can now be integrated with respect to the transformed coordinate φ across the two boundary layers. The integration yields:

$$\int_{\varphi(\sigma_1)}^{\varphi(y)} \frac{\partial c}{\partial t}\, d\varphi = \int_{\varphi(\sigma_1)}^{\varphi(y)} \lambda(x) \frac{\partial^2 c}{\partial \varphi^2}\, d\varphi, \quad \epsilon < x < y \tag{II.32a}$$

$$\int_{\varphi(y)}^{\varphi(\sigma_2)} \frac{\partial c}{\partial t}\, d\varphi = \int_{\varphi(y)}^{\varphi(\sigma_2)} \lambda(x) \frac{\partial^2 c}{\partial \varphi^2}\, d\varphi, \quad y < x < 1-\epsilon. \tag{II.32b}$$

After application of Leibnitz's rule on the left hand side, substitution of (II.19) on the right hand side and simplification, equations (II.32a,b) become:

$$\frac{d}{dt}\int_{\varphi(\sigma_1)}^{\varphi(\gamma)} c\,d\varphi = 2a_3\int_{\sigma_1}^{\gamma}\lambda^2(x)\,dx, \qquad \epsilon < x < \gamma \tag{II.33a}$$

$$\frac{d}{dt}\int_{\varphi(\gamma)}^{\varphi(\sigma_2)} c\,d\varphi = 2a_6\int_{\gamma}^{\sigma_2}\lambda^2(x)\,dx, \quad \gamma < x < 1-\epsilon. \tag{II.33b}$$

When equations (II.29) through (II.31) are substituted in equations (II.33a,b) the following sets of ordinary differential equations result:

$0 \le t \le t_1$:

$$\frac{d\sigma_1}{dt} = \Big\{3\big[(\gamma(\sigma_2)-\gamma(\gamma))(\varphi(\sigma_1)-\varphi(\gamma))^4 - (\gamma(\gamma)-\gamma(\sigma_1))(\varphi(\gamma)-\varphi(\sigma_2))^3 (2\varphi(\sigma_1)-\varphi(\sigma_2)-\varphi(\gamma))\big]\Big\} \Big/ \Big\{(\varphi(\sigma_1)-\varphi(\sigma_2))(\varphi(\sigma_1)-\varphi(\gamma))^2(\varphi(\gamma)-\varphi(\sigma_2))^3\Big(\beta+\frac{\theta a}{\sigma_1(1-\sigma_1)}\Big)\Big\} \tag{II.34a}$$

$$\frac{d\sigma_2}{dt} = \Big\{3\big[(\gamma(\sigma_2)-\gamma(\gamma))(\varphi(\sigma_1)-\varphi(\gamma))^3(\varphi(\sigma_1)-2\varphi(\sigma_2)+\varphi(\gamma)) - (\gamma(\gamma)-\gamma(\sigma_1))(\varphi(\gamma)-\varphi(\sigma_2))^4\big]\Big\} \Big/ \Big\{(\varphi(\sigma_1)-\varphi(\sigma_2))(\varphi(\gamma)-\varphi(\sigma_2))^2(\varphi(\sigma_1)-\varphi(\gamma))^3\Big(\beta+\frac{\theta a}{\sigma_2(1-\sigma_2)}\Big)\Big\} \tag{II.34b}$$

where at t = 0

$$\sigma_1(0) = \sigma_2(0) = y \qquad \text{(II.34c)}$$

$t_1 \leq t \leq t_2$:

$$\frac{d\alpha_1}{dt} = 3\{[(\alpha_1+1)(\varphi(y)-\varphi(\sigma_2))+2\alpha_1\varphi(\sigma_2)](\gamma(y)-\gamma(\epsilon))$$
$$(\varphi(\sigma_2)+\varphi(y))(\varphi(\sigma_2)-\varphi(y))^2+(\alpha_1+1)(\gamma(\sigma_2)-\gamma(y))\varphi^4(y)\}/$$
$$\{(\varphi(\sigma_2)-\varphi(y))^2\varphi^2(\sigma_2)\varphi^3(y)\}$$

(II.35a)

$$\frac{d\sigma_2}{dt} = 3\{(\alpha_1+1)(\gamma(\sigma_2)-\gamma(y))\varphi^3(y)(\varphi(y)-2\varphi(\sigma_2))$$
$$-[(\alpha_1+1)(\varphi(y)-\varphi(\sigma_2))+2\alpha_1\varphi(\sigma_2)](\gamma(y)-\gamma(\epsilon))$$
$$(\varphi(\sigma_2)-\varphi(y))^3\}/\{(\beta+\frac{\Theta a}{\sigma_2(1-\sigma_2)})(\varphi(\sigma_2)-\varphi(y))^2$$
$$\varphi(\sigma_2)(\alpha_1+1)\varphi^3(y)\}$$

(II.35b)

where at $t = t_1$

$$\alpha_1(t_1) = 0 \qquad \text{(II.35c)}$$

For $t_2 \leq t \leq t_\infty$:

$$\frac{d\alpha_1}{dt} = 3\phi\Big\{\big[(\varphi(1-\epsilon)-\varphi(y))(1+\alpha_1-\alpha_2)-2\alpha_1\varphi(1-\epsilon)\big](\gamma(y)-\gamma(\epsilon))$$
$$(\varphi(y)+\varphi(1-\epsilon))(\varphi(1-\epsilon)-\varphi(y))^2+\big[\varphi(y)(1+\alpha_1-\alpha_2)$$
$$+2\alpha_2\varphi(1-\epsilon)\big](\gamma(y)-\gamma(\epsilon))\varphi^3(y)\Big\}\Big/\big[\varphi^2(1-\epsilon)$$
$$(\varphi(1-\epsilon)-\varphi(y))^2\big] \tag{II.36a}$$

$$\frac{d\alpha_2}{dt} = 3\phi\Big\{\big[\varphi(y)(1+\alpha_1-\alpha_2)-2\varphi(1-\epsilon)\alpha_2\big](\gamma(y)-\gamma(\epsilon))$$
$$(2\varphi(1-\epsilon)-\varphi(y))\varphi^2(y)+\big[(\varphi(1-\epsilon)-\varphi(y))(1+\alpha_1-\alpha_2)$$
$$-2\alpha_1\varphi(1-\epsilon)\big](\gamma(y)-\gamma(\epsilon))(\varphi(1-\epsilon)-\varphi(y))^3\varphi\Big/$$
$$\phi\big(\varphi(1-\epsilon)-\varphi(y)\big)^3\varphi^2(1-\epsilon)\varphi^2(y)\varphi \tag{II.36b}$$

and at $t = t_2$

$$\alpha_2(t_2) = 0 \tag{II.36c}$$

and

$$\gamma(x) = \phi\Big\{\beta^2 x + 2\theta a\beta \ln\Big[\frac{x}{1-x}\Big] + \theta^2 a^2\Big[\frac{2x-1}{x(1-x)} + 2\ln\Big[\frac{x}{1-x}\Big]\Big]\Big\} \tag{II.37}$$

The above coupled non-linear differential equations have been solved numerically. The only difficulty arises at t = 0 where both d σ_1/dt and d σ_2/dt are singular in equations (II.34a,b). To circumvent this difficulty one constructs an analytic solution valid for short times as outlined below.

One first substitutes the concentration profile (II.29a) in the integral relation (II.33a):

$$-\frac{d}{dt}\left[c(\varphi(y),t)(\varphi(\sigma_1)-\varphi(y))\right] = \frac{6\,c(\varphi(y),t)(\gamma(y)-\gamma(\sigma_1))}{(\varphi(\sigma_1)-\varphi(y))^2} \qquad \text{(II.38)}$$

and rewrites equation (II.38) in the form:

$$-\frac{d\varphi(\sigma_1)}{dt}+\frac{\varphi(y)-\varphi(\sigma_1)}{c(\varphi(y),t)}\frac{dc(\varphi(y),t)}{dt} = \frac{6(\gamma(y)-\gamma(\sigma_1))}{(\varphi(\sigma_1)-\varphi(y))^2} \qquad \text{(II.39)}$$

Combining equations (II.20), (II.29a) and (II.29c) one obtains:

$$\frac{1}{c(\varphi(y),t)}\frac{dc(\varphi(y),t)}{dt} = \frac{2\lambda(x)}{(\varphi(\sigma_1)-\varphi(x))^2}$$

$$-2\left(\frac{\varphi(x)-\varphi(y)}{\varphi(\sigma_1)-\varphi(y)}\right)\frac{1}{\varphi(\sigma_1)-\varphi(x)}\frac{d\varphi(\sigma_1)}{dt} \qquad \text{(II.40)}$$

Noting that as $t \to 0$, $\sigma_1 \to y$ and substituting (II.40) in (II.39), one finds that

$$\lim_{\sigma_1 \to \gamma} \frac{d\,g(\sigma_1)}{dt} = -2 \lim_{\sigma_1 \to \gamma} \left[\frac{\sigma(\gamma) - \sigma(\sigma_1)}{(g(\sigma_1) - g(\gamma))^2} \right] . \tag{II.41}$$

The right hand side of (II.41) is evaluated using L'Hospital's rule. The desired equation for $t \ll 1$ is

$$\frac{d\sigma_1}{dt} = \frac{1}{\beta(\sigma_1 - \gamma) + \theta a \ln\left(\frac{\sigma_1}{1-\sigma_1} \cdot \frac{1-\gamma}{\gamma}\right)} . \tag{II.42}$$

After integration and simplification, one can show from (II.42) that for very short times:

$$\sigma_1 = \gamma - \sqrt{\frac{t}{\beta/2 + \frac{\theta a}{\gamma(1-\gamma)}}} \quad , \quad t \ll 1 . \tag{II.43}$$

In a similar manner σ_2 is found to be:

$$\sigma_2 = \gamma + \sqrt{\frac{t}{\beta/2 + \frac{\theta a}{\gamma(1-\gamma)}}} \quad , \quad t \ll 1 . \tag{II.44}$$

The unknown function A(t) in the solution for the vesicle density distribution near the plasmalemma can now be determined by matching the behavior of the near field solution (II.13) for large values of (x/ϵ_0) with the behavior of (II.21a) as x approaches ϵ. The value of A(t) determined in this manner is:

$$A(t) = \alpha_1(t)\,\phi\,\ell \, , \tag{II.45}$$

where $\alpha_1(t)$ is determined from the numerical integration of equations (II.35a) and (II.36a).

One can also show from equations (II.24) and (II.29) through (II.31) that the fraction ϕ_L/ϕ of the vesicles that return to the luminal membrane and the fraction ϕ_R/ϕ that are transported across the cell are given by :

$0 \le t \le t_1$:

$$\frac{\phi_L}{\phi} = \frac{\psi(\gamma) - \psi(\sigma_2)}{\psi(\sigma_1) - \psi(\sigma_2)} \qquad \text{(II.46a)}$$

$$\frac{\phi_R}{\phi} = \frac{\psi(\sigma_1) - \psi(\gamma)}{\psi(\sigma_1) - \psi(\sigma_2)} \qquad \text{(II.46b)}$$

$t_1 \le t \le t_2$:

$$\frac{\phi_L}{\phi} = \frac{\psi(\sigma_2) - \psi(\gamma)}{\psi(\sigma_2)} - \frac{\alpha_1 \psi(\gamma)}{\psi(\sigma_2)} \qquad \text{(II.47a)}$$

$$\frac{\phi_R}{\phi} = \frac{(\alpha_1 + 1)\psi(\gamma)}{\psi(\sigma_2)} \qquad \text{(II.47b)}$$

$t_2 \le t \le t_\infty$:

$$\frac{\phi_L}{\phi} = (1 - \alpha_2)\left(\frac{\psi(1-\epsilon) - \psi(\gamma)}{\psi(1-\epsilon)}\right) - \alpha_1 \frac{\psi(\gamma)}{\psi(1-\epsilon)} \qquad \text{(II.48a)}$$

$$\frac{\phi_R}{\phi} = \alpha_2 + (1 + \alpha_1 - \alpha_2)\frac{\psi(\gamma)}{\psi(1-\epsilon)} \; . \qquad \text{(II.48b)}$$

In the steady state the transient term in equation (II.20) disappears. Integration of the resulting equation gives:

$$c_1 = b_1 + b_2 \varphi, \quad x < y \tag{II.49a}$$

$$c_2 = b_3 + b_4 \varphi, \quad x > y. \tag{II.49b}$$

The four unknown coefficients b_i, $i = 1...4$, are determined by the transformed boundary and matching conditions (II.22) through (II.24) which are also independent of λ. The resulting steady state concentration profiles in φ space are:

$$c(\varphi(x)) = [1 - \varphi(y)/\varphi(1-\epsilon)]\varphi(x), \quad \epsilon \le x \le y \tag{II.50a}$$

$$c(\varphi(x)) = [1 - \varphi(x)/\varphi(1-\epsilon)]\varphi(y), \quad y \le x \le 1-\epsilon. \tag{II.50b}$$

These profiles are valid for an arbitrary hydrodynamic resistance law in the cell interior. The resistance law is entirely contained in the coordinate transformation (II.19) relating φ and x.

One can readily show that if θ and β in (II.9) are chosen to be unity, equations (II.50a,b) are identical to the steady state solutions (3.25a,b) in Weinbaum and Caro (1976).

The steady state vesicle flux ratios are easily found using equations (II.24) and (II.50a,b):

$$\frac{\phi_2}{\phi} = 1 - \frac{\varphi(y)}{\varphi(1-\epsilon)} \tag{II.51a}$$

$$\frac{\phi_R}{\phi} = \frac{\mathcal{S}(\gamma)}{\mathcal{S}(1-\epsilon)} \qquad \text{(II.51b)}$$

II-3b. Steady State Permeability

The steady state permeability of the endothelial cell layer is defined by the expression:

$$P = J/(c_p - c(0)), \qquad \text{(II.52)}$$

where c_p and $c(0)$ are the dimensional macromolecule concentrations at the luminal and interstitial surface of the endothelial cell layer respectively and J is the net macromolecule flux across the endothelium due to vesicle transport.

If V is the internal volume of the vesicles then the net macromolecule flux can be written as:

$$J = \phi_R V (c_p - c(0)). \qquad \text{(II.53)}$$

The preceding expression for J assumes that the vesicle attachment time t_a is long compared to the time that it takes the macromolecules to achieve concentration equilibrium with the luminal fluid. Experiments with large tracer molecules, such as ferritin (Casley-Smith and Chin, 1971; Clough and Michel, 1978) strongly suggest that molecular sieving effects may play an important role in vesicle

filling. This effect is easily accounted for in the present analysis by multiplying the above expression for J by an exponential factor $\exp(-t_f/t_a)$ which describes a diffusion barrier with characteristic passage time t_f at the mouth of the vesicle.

Combining (II.52), (II.53) and (II.51b), one has:

$$P = \frac{\phi V \vartheta(\gamma)}{\vartheta(1-\epsilon)} \quad , \tag{II.54}$$

where the vesicle release rate ϕ can be expressed in terms of the number density of attached vesicles N_a and the average attachment time of a vesicle t_a as:

$$\phi = N_a / t_a \quad . \tag{II.55}$$

From equation (II.1) t_a is given by:

$$t_a = \frac{1}{k_1^d} + \frac{1}{k_{-1}^d} \quad . \tag{II.56}$$

Equation (II.56) states that the attachment time is equal to the sum of the time for the vesicle to be released from its open attached configuration plus the time required for the vesicle to undergo the transition from sketch (c) to the open attached state for sketch (d) in Fig. II.1.

The total vesicle population N per unit area of endothelial surface is defined as $N \equiv 2N_a + N_f$ where

N_f is the number of free vesicles per unit area of endothelial surface. The expression for N_f can be non-dimensionalized as:

$$N_f^* = \frac{N_f D_o}{\phi \ell^2} \tag{II.57}$$

N_f^* is found by integration of the dimensionless concentration profile across the cell:

$$N_f^* = \int_0^{\varphi(1-\epsilon)} c \, d\varphi \, . \tag{II.58}$$

Substitution of (II.50a,b) for c in (II.58) leads to:

$$N_f^* = \frac{1}{2} \left(\varphi(1-\epsilon) - \varphi(Y) \right) \varphi(Y) \, . \tag{II.59}$$

When the defintion of N is combined with (II.55) to (II.57), one obtains the following relation for ϕ :

$$\phi = \frac{N}{2\left(\frac{1}{\kappa_1^d} + \frac{1}{\kappa_{-1}^d}\right) + \frac{\ell^2}{D_o} N_f^*} \tag{II.60}$$

Substitution of (II.60) in (II.54) gives the desired expression for the steady state permeability:

$$P = \frac{NV}{2} \frac{\varphi(Y)}{\varphi(1-\epsilon)} \left[\frac{\kappa_1^d}{\left(1 + \frac{\kappa_1^d}{\kappa_{-1}^d}\right) + \frac{\ell^2 N_f^* \kappa_1^d}{2 D_o}} \right] \tag{II.61}$$

Equation (II.61) is valid for an arbitrary hydrodynamic resistance law $\lambda(x)$.

Since open attached vesicles are found more than a hundred times more frequently than the double applanated membrane geometry, the electron micrographs of Palade and Bruns (1968) suggest that the residence time in the open attached configuration is much longer than the time for the dissolution of the double applanated membrane in sketch (c) of Fig. II.1; thus, $k_1^d \ll k_{-1}^d$. This is in contrast to Rubin (1977) where the attachment/detachment processes are considered to be a mirror image sequence of events. Assuming the last inequality valid, one obtains the following approximate relation for the steady state permeability:

$$P = \frac{N V K_1^d}{2} \frac{\mathcal{Y}(y)}{\mathcal{Y}(1-\epsilon)} \left[\frac{1}{1 + \frac{\ell^2 N_f^* K_1^d}{2 D_0}} \right] . \quad \text{(II.62)}$$

Two dimensionless parameters appear in equation (II.62), $\mathcal{Y}(y)/\mathcal{Y}(1-\epsilon)$ and $\ell^2 k_1^d / 2D_0$: The first from equation (II.51b) describes the probability that a vesicle released at x = y will diffuse across the cell. The second parameter is a characteristic number describing the ratio of vesicle diffusion to attachment times. N_f^* has been separated out in forming this ratio since it is a function of ϵ from equation (II.59). Equations (II.61) or (II.62) are the generalization of Rubin's constant diffusivity steady state permeability analysis to an arbitrary one-dimensional spatial variation of diffusivity in the cell interior.

II-4. RESULTS

Section II-4a presents results to the transient concentration profiles and vesicle flux ratios derived in section II-3a. In section II-4b the results for steady state permeability derived in section II-3b. are presented.

II-4a. Results for Vesicle Concentration and Flux

Equations (II.34) to (II.36) were solved using a fourth order Runge-Kutta procedure. Average computation times were about 90 seconds on an AMDAHL 470/V6 computer.

The time dependent dimensionless concentration profiles given by (II.29) to (II.31) are plotted for effective van der Waals cut-off distances of 15 Å and 100 Å in Figs. II.4 and II.5. The time dependent flux ratios given by equations (II.46) to (II.48) are plotted in Fig. II.6 for four representative values of ϵ.

To compare the predictions of the theory with the time dependent tracer studies of Casley-Smith and Chin (1971) one needs to determine the proportion of labelled vesicles to total concentration of vesicles at any distance across the endothelium. The total concentration at any point, because of the symmetry of the transport is obtained by simply adding the steady state concentration profiles due to vesicle release at both the lumen and tissue fronts. The steady state profile for vesicles released at the luminal front is given by equations (II.50a,b). The corresponding expressions for the vesicles released at

the tissue front are:

$$c(\varphi(x)) = \left[1 - \frac{\varphi(1-y)}{\varphi(1-\epsilon)}\right]\varphi(x), \quad \epsilon \leq x \leq 1-y \qquad \text{(II.63a)}$$

$$c(\varphi(x)) = \left[1 - \frac{\varphi(x)}{\varphi(1-\epsilon)}\right]\varphi(1-y), \quad 1-y \leq x \leq 1-\epsilon. \qquad \text{(II.63b)}$$

The theoretical curves for the proportion of labelled vesicles and the experimental data of Casley-Smith and Chin are shown in Fig. II.7. For the comparison the transendothelial diffusion distance was assumed to be 4300 Å and the van der Waals cut-off distance 15 Å.

II-4b. Results for Steady State Permeability

The steady state permeability approximated by equation (II.62) is plotted in dimensionless form in Fig. II.8 as a function of van der Waals cut-off distance for different values of the dimensionless number $\ell^2 k_1^d/2D_0$ characterizing the ratio of diffusion to attachment time. $2P/NVk_1^d$ is a dimensionless permeability coefficient. Fig. II.9 is a cross-plot of Fig. II.8 for van der Waals cut-off distances of 15 Å, 25 Å and 100 Å.

II-5. DISCUSSION

The concentration profiles of Figs. II.4 and II.5 show similar qualitative behavior. For short times ($t^* \lesssim 10^{-3}$) the concentration profiles on each side of the plane of release are identical. This occurs because the vesicles have not moved far enough from x = y to see a difference in hydrodynamic resistance due to the luminal plasmalemma. The growth of the boundary layers, which is initially symmetric, becomes asymmetric as the vesicles approach the luminal plasmalemma, where the transition from the first to the second time scale occurs. This behavior can be seen in both figures but occurs at an earlier time in Fig. II.5 where the van der Waals cut-off distance is closer to the vesicle plane of release. The concentration of free vesicles at any given time is seen to be substantially larger for the smaller van der Waals cut-off distance (ϵ_0 = 15 Å) because vesicle reattachment at the luminal plasmalemma is less likely to occur the further ϵ is removed from x = y. One can see a continued growth of the rightward moving boundary layer until t^* is of $O(10^{-1})$. This is where the transition from the second to third time scale occurs. During the third time scale there is a continued increase in the labelled free vesicle population until a steady state is achieved. If the time to reach steady state is taken to be the time at which the peak concentration of labelled vesicles has reached 98% of its final value, then t^*_∞ = 0.170 and 0.111 for ϵ_0 = 15 Å and 100 Å respectively.

Thus, ϵ has only a small effect on the time to achieve a steady state, but has a significant effect on the number of free vesicles (area under the concentration curves) in the steady state.

From equation (II.11) the dimensionless and actual times are related by $t = t^* \ell^2/D_0$. In order to calculate D_0 from the Stokes-Einstein relation, one needs to know the intracellular viscosity. Unfortunately, there is a great deal of uncertainty in the value of this physical quantity. Values in the literature range from 0.2 poise (Casley-Smith and Chin, 1971) to 8 poise (Shea, Karnovsky and Bossert, 1969) and higher.

Casley-Smith and Chin (1971) found experimentally that it took roughly 10 sec for a steady state to be reached. Using this value for the equilibration time and the previously stated criterion for determining t^*_∞, one is able to estimate the value of the intracellular viscosity from the definition of t^* and the Stokes-Einstein relation. For a transendothelial diffusion distance of 4300 $\mathring{A}$ at 37°C, one obtains an approximate value for μ_0 of 8.9 poise.

The flux ratios in Fig. II.6 show two interesting features. First, as discussed previously in connection with Figs. II.4 and II.5, the probability that a vesicle will cross the cell layer ϕ_R/ϕ increases as ϵ decreases since a vesicle is less likely to reattach at the same surface from which it was released the further ϵ is removed from the release plane x = y. Second, the curves of

Fig. II.6 exhibit a maximum for dimensionless times of $O(10^{-2})$. This behavior can be explained as follows. For very small dimensionless times ($t^* < O(10^{-3})$) a vesicle experiences little difference in hydrodynamic resistance on either side of x = y since it is very close to the release plane and the solution, as one observes from equations (II.43) and (II.44), is initially symmetric and independent of ϵ; thus, $\phi_R/\phi \approx 0.5$. As time proceeds, the presence of the luminal plasmalemma increases the hydrodynamic resistance for the boundary layer growing toward the left ($x < y$) and the vesicle flux increases preferentially toward the tissue side. This behavior continues until the rightward growing boundary layer ($x > y$) starts to encounter the increased hydrodynamic resistance offered by the plasmalemma membrane on the tissue side (see Figs. II.4 and II.5). The vesicle flux toward the tissue front now starts to decrease until at dimensionless times of O(1) a steady state is established.

Fig. II.7 shows only fair agreement between the theoretically predicted concentration profiles and the experimental data of Casley-Smith and Chin (1971). The discrepancy is most noticeable close to the plasmalemma membranes. A reasonable explanation for this difference is the steric hindrance of attached vesicles which has been neglected in this model. A free vesicle attempting to attach at a plasmalemma membrane experiences both a steric exclusion and increased hydrodynamic resistance. This effect would

increase the concentration gradient in the regions near the plasmalemma membranes while decreasing the gradient in the interior, as observed in the experimental data. Also, the data of Casley-Smith and Chin should be cautiously interpreted since it is extremely difficult to distinguish an attached from a free vesicle when close to the plasmalemma if the location of the cutting plane is not known.

Fig. II.8 shows the effect of the van der Waals cut-off distance ϵ on the steady state permeability of the endothelial cell layer for several representative values of the dimensionless number $\ell^2 k_1^d / 2D_0$. One observes that the permeability is a sensitive function of ϵ when the attachment time is rate-controlling ($\ell^2 k_1^d / 2D_0 << 1$) and is relatively insensitive to ϵ when the diffusion time is rate-controlling ($\ell^2 k_1^d / 2D_0 >> 1$). When $\ell^2 k_1^d / 2D_0 << 1$ the dimensionless permeability coefficient depends primarily on the factor $\varphi(y)/\varphi(1-\epsilon)$ in equation (II.62) describing the probability that a vesicle released at the luminal plasmalemma will cross to the other side of the cell. This probability decreases as the van der Waals cut-off distance increases for the reasons stated previously. When $\ell^2 k_1^d / 2D_0 >> 1$ two opposing effects are present as ϵ is increased. While the probability that a vesicle crosses the endothelial cell decreases, the number of free vesicles in the diffusion region N_f^* decreases, increasing the number of attached vesicles and hence the vesicle release rate. These two effects nearly cancel one another producing a permeability

coefficient that is nearly independent of ϵ.

In Fig. II.9 the dimensionless permeability coefficient is plotted as a function of $\ell^2 k_1^d / 2D_0$ for several representative values of ϵ. The behavior of the steady state permeability coefficient in the two limits just described is clearly shown in this figure. The other feature of the curves in Fig. II.9, which is not evident from Fig. II.8, is that the permeability coefficient is a rapidly varying function of $\ell^2 k_1^d / 2D_0$ when this dimensionless time ratio is of O(1) or smaller and a slowly varying function for large values of this dimensionless number.

The dimensionless concentration profiles, flux ratios and permeability described above are all independent of intracellular viscosity. This is an important result since as noted previously there is considerable uncertainty in the actual value of μ_0 and hence D_0.

In this chapter a time dependent vesicle labelling theory has been presented which includes the spatial dependence of hydrodynamic and electrodynamic forces produced by both plasmalemma membranes and which is valid for all time. Chapter 3 will be concerned with an improvement of the accuracy of the mathematical model by taking account of the steric hindrance and increased hydrodynamic resistance of a free vesicle near a plasmalemma due to the presence of already attached vesicles.

Table II.1. Comparison of approximate expressions (II.9) and (3.23) of Weinbaum and Caro (1976) with exact expression (Ganatos, Weinbaum and Pfeffer, 1979) for hydrodynamic interaction parameter for perpendicular motion of a spherical particle between two walls.
$a/\ell = 0.14$, $\alpha = 1.036$, $\beta = 0.915$.

x/ℓ	λ exact (Ganatos et al.)	λ approx. equation (II.9)	λ approx. (Weinbaum and Caro)
0.01	15.52	15.54	15.14
0.05	4.058	3.963	3.947
0.1	2.5712	2.5239	2.5556
0.2	1.8158	1.8201	1.8750
0.3	1.5750	1.6046	1.6667
0.4	1.4762	1.5184	1.5833
0.5	1.4481	1.4943	1.5600

CHAPTER II. NOMENCLATURE

a	vesicle radius
a_i	coefficients of polynomial profile for transient vesicle number density i = 1,...6
$A(t^*)$	function defined by (II.13)
b_i	coefficients of polynomial profile for steady state vesicle number density i = 1,...4
c	vesicle number density
c_p	dimensional macromolecule concentration at luminal surface
c_T	total vesicle number density at any location across endothelial cell
$c(0)$	dimensional macromolecule concentration at interstitial surface
c^*	scaled vesicle number density $c^* = cD_0/\phi\ell^2$
c'	speed of propagation of an elastic wave in a flexible tube of radius R
$D(x)$	spatially varying diffusion coefficient
D_0	unbounded vesicle diffusion coefficient
E	Young's modulus
$\Delta G^d_{\pm i}$	free energy of activation associated with the formation or rupture of the membrane diaphragm of an attached vesicle (i refers to region where reaction is taking place and $\pm$ indicates direction of reaction with respect to x coordinate)
h	Planck's constant
h'	membrane bilayer thickness
J	net macromolecule flux across endothelium due to vesicle transport
k	Boltzmann's constant
$k^d_{\pm i}$	rate constant describing velocity of reaction associated with the formation or rupture of the membrane diaphragm of an attached vesicle (i refers to region where reaction is taking place and $\pm$ indicates direction with respect to x coordinate)

$k_{\pm i}^{o,d}$	reaction rate constant according to absolute reaction rate theory (i refers to region where reaction is taking place and $\pm$ indicates direction with respect to x coordinate
ℓ	transendothelial diffusion distance
N	total vesicle population per unit area of endothelial surface $N \equiv 2N_a + N_f$
N_a	number of attached vesicles per unit area of endothelial surface
N_f	number of free vesicles per unit area of endothelial surface
N_f^*	scaled number of free vesicles per unit area of endothelial surface $N_f^* = N_f D_0/\phi\ell^2$
P	steady state permeability
r	radial distance
R	vesicle neck radius
$\mathcal{R}$	molar gas constant
t	time
t^*	scaled time $t^* = tD_0/\ell^2$
t_a	vesicle attachment time
t_f	vesicle filling time
T	temperature
u_{vw}	convective velocity for vesicle created by van der Waals force
u_{vw}^*	scaled convective velocity $u_{vw}^* = u_{vw}a/D_0$
V	internal volume of vesicle
w(r-a,t)	probability that any portion of the vesicle membrane will be located in a spherical shell of thickness dr at a distance r-a from its initial position r = a at t = 0
x	distance coordinate
x^*	scaled distance coordinate $x^* = x/\epsilon_0$ or x/ℓ

x_e amplitude of individual thermal excursion

y vesicle plane of release

α_1 concentration gradient at edge of left boundary layer ($x < y$)

α_2 concentration gradient at edge of right boundary layer ($x > y$)

β correction for combined interaction of walls

$\gamma(x)$ function defined by (II.37)

δ_1 boundary layer thickness left of vesicle plane of release ($x < y$)

δ_2 boundary layer thickness right of vesicle plane of release ($x > y$)

ϵ dimensionless cut-off distance of van der Waals force $\epsilon = \epsilon_0/\ell$

ϵ_0 effective London-van der Waals cut-off distance

η transformed distance coordinate

θ correction to Taylor lubricating film resistance

λ hydrodynamic interaction parameter describing the variation in fluid resistance for the perpendicular motion of a spherical particle between two parallel walls

λ' wavelength of wave in neck region

$\lambda_i^{o,d}$ length of the reaction zone traversed between initial and final state configurations in formation or rupture of the membrane diaphragm of an attached vesicle

μ viscosity

μ_0 actual fluid viscosity (unbounded medium)

σ_1 distance from origin to left boundary layer edge ($x < y$)

σ_2 distance from origin to right boundary layer edge ($x > y$)

ϕ vesicle release rate per unit area of endothelial surface

ϕ_L/ϕ fraction of vesicles that return to luminal membrane

ϕ_R/ϕ fraction of vesicles transported across cell

$\chi^d_{\pm i}$ transmission coefficient (i refers to region where reaction is taking place and $\pm$ indicates direction with respect to x coordinate)

ω wave frequency

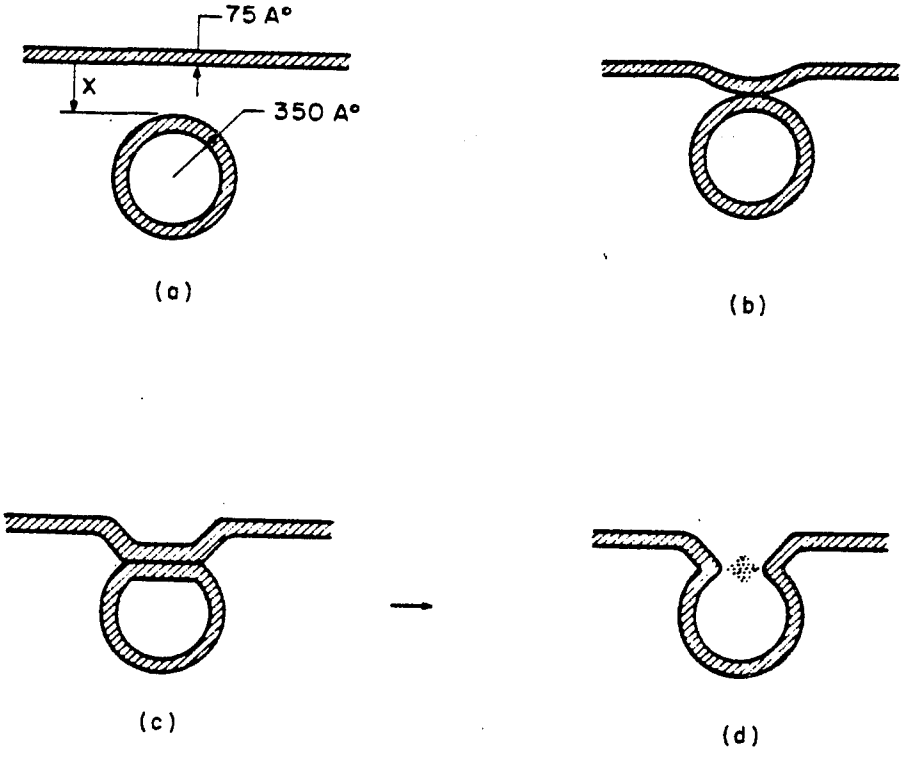

Figure II.1. Sketch of proposed sequence of events leading to reattachment of free vesicles to plasmalemma membrane. (a) $x > 200$ Å, hydrodynamic interaction. (b) $x < 200$ Å, hydrodynamic-van der Waals interaction. (c) Before stalk formation. (d) Reattached configuration.

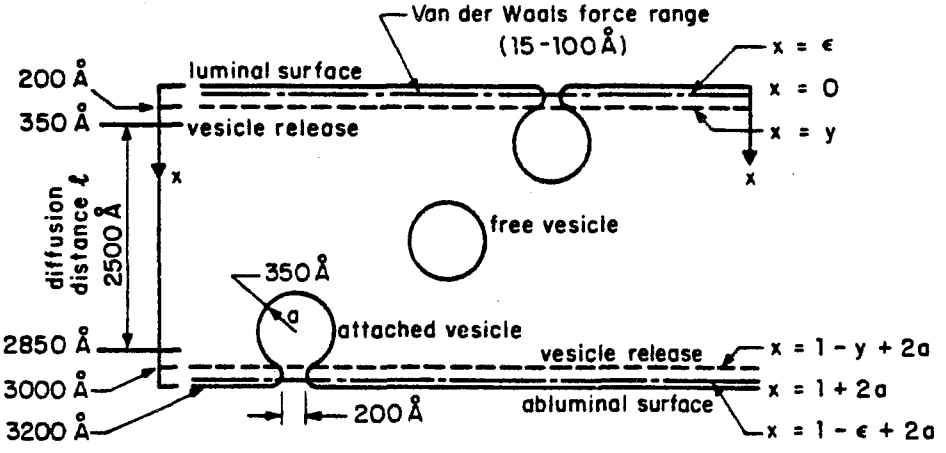

Figure II.2. Schematic illustration showing coordinates and geometry for mathematical model of plasmalemma vesicle migration across border region of endothelial cell. Dimensions based on canine carotid artery.

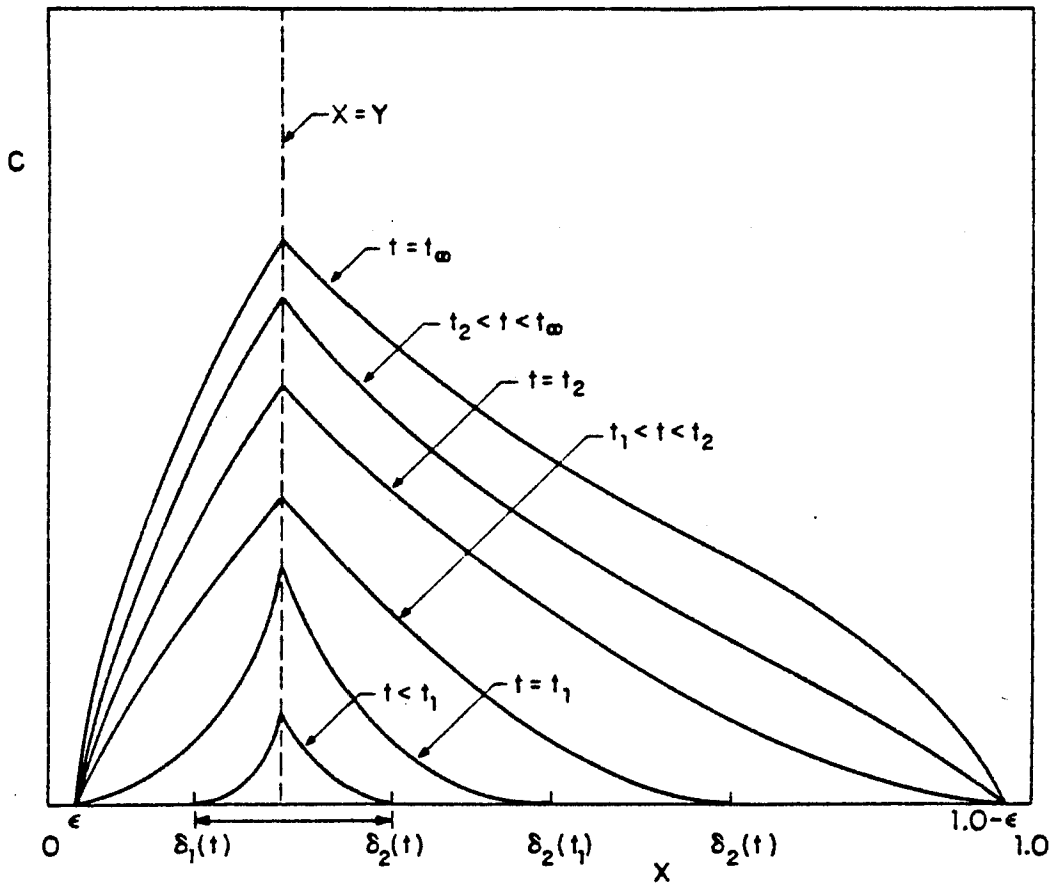

Figure II.3. Three time domains for concentration profiles of integral solution technique.

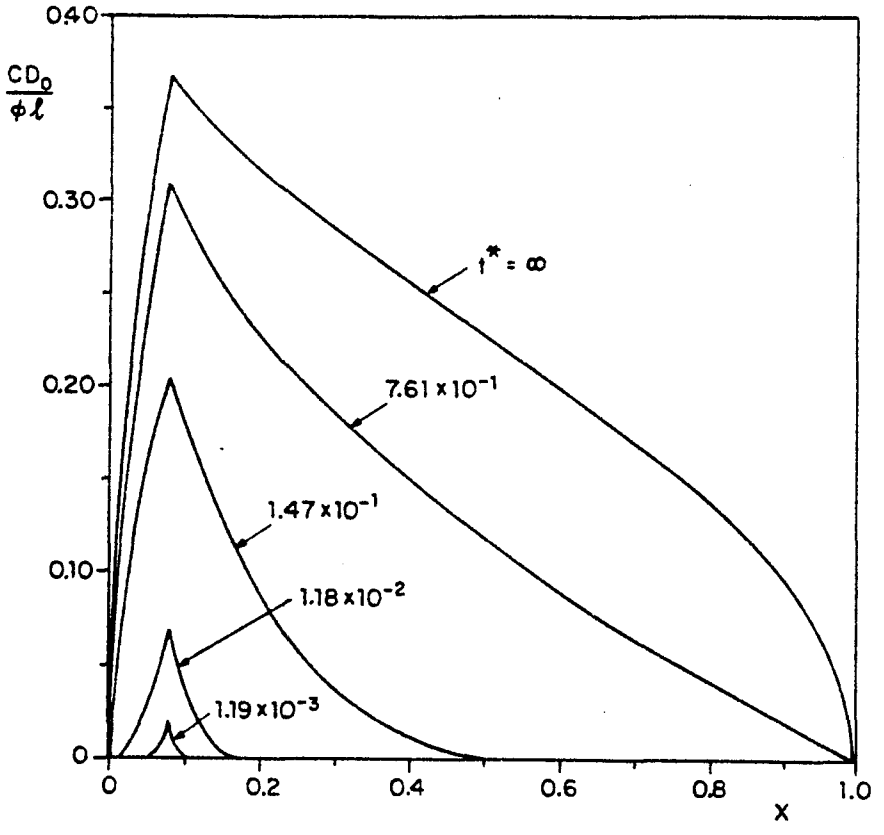

Figure II.4. Theoretical time dependent concentration distribution of free vesicles released at luminal membrane for an effective van der Waals cut-off distance ϵ_0 of 15 Å and a transendothelial diffusion distance ℓ of 2500 Å.

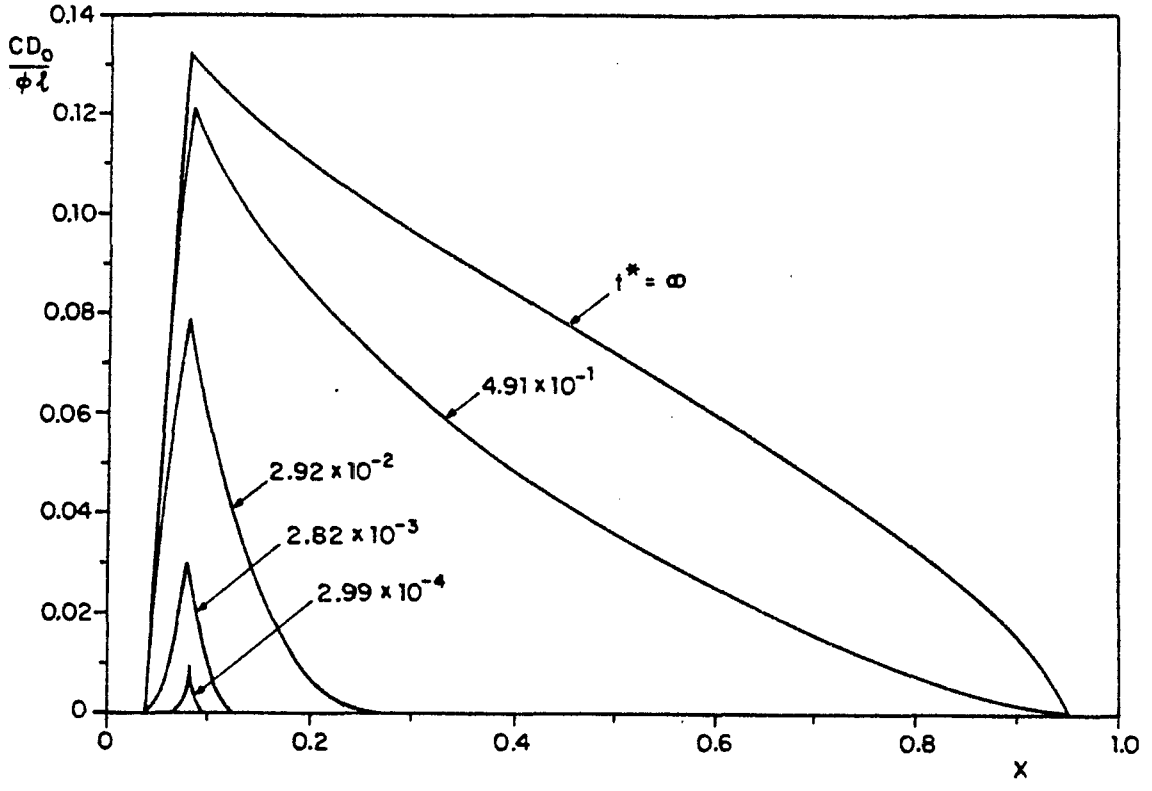

Figure II.5. Theoretical time dependent concentration distribution of free vesicles released at luminal membrane for an effective van der Waals cut-off distance ϵ_0 of 100 Å and a transendothelial diffusion distance ℓ of 2500 Å.

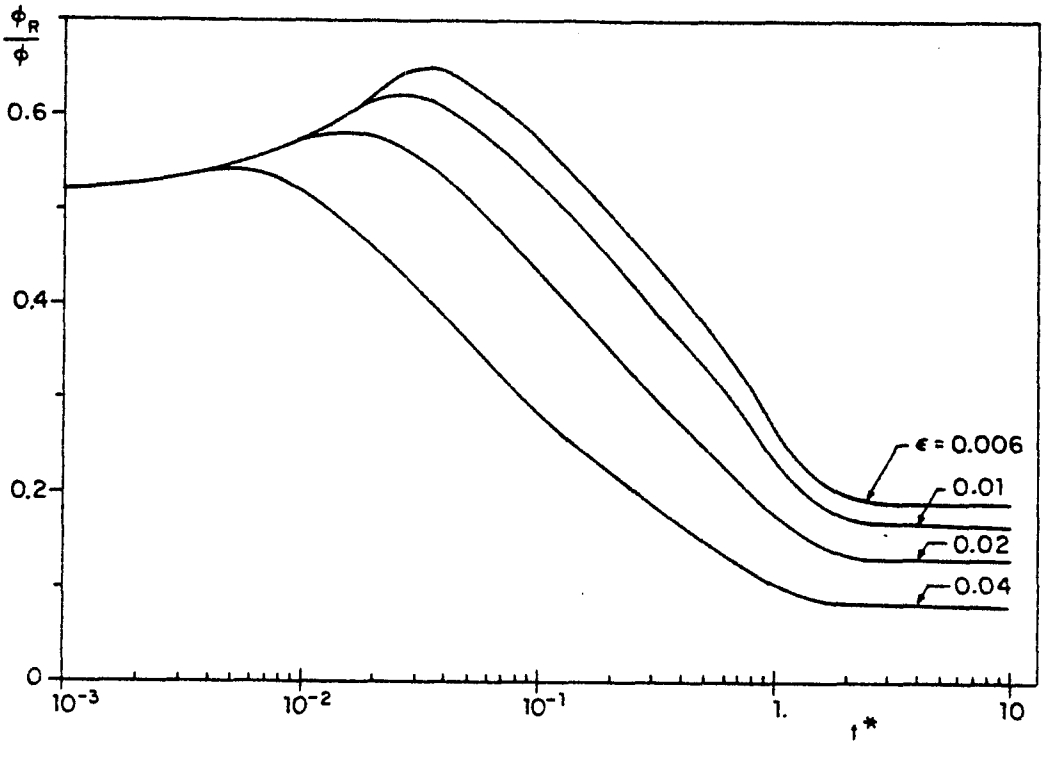

Figure II.6. Theoretical time dependent solution for fractional flux ϕ_R/ϕ of vesicles crossing the cell for representative values of the effective van der Waals cut-off distance ϵ where the transendothelial diffusion distance ℓ is 2500 Å.

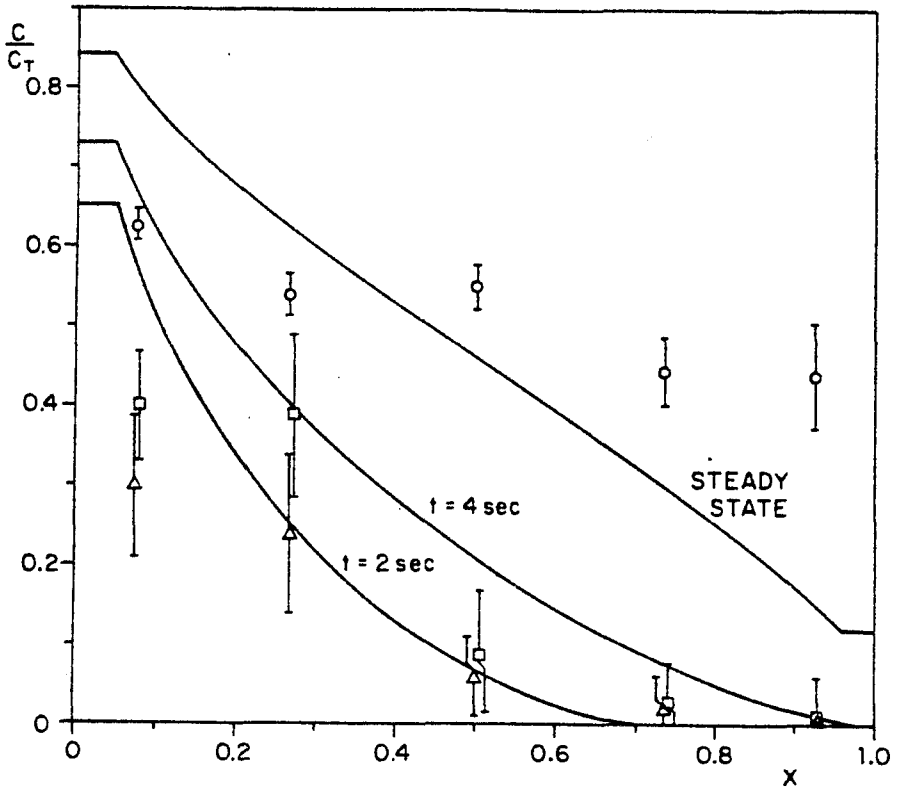

Figure II.7. Theoretical and experimental time dependent proportion of labeled vesicles c/c_T as a function of distance x for an effective van der Waals cut-off distance ϵ_0 of 15 Å and a transendothelial diffusion distance ℓ of 4300 Å. Experimental data, Δ, 2s; □, 4s; o ≥ 16s (Casley-Smith and Chin, 1971: vesicles labeled with horseradish peroxidase). Vertical bars represent ±1 standard error.

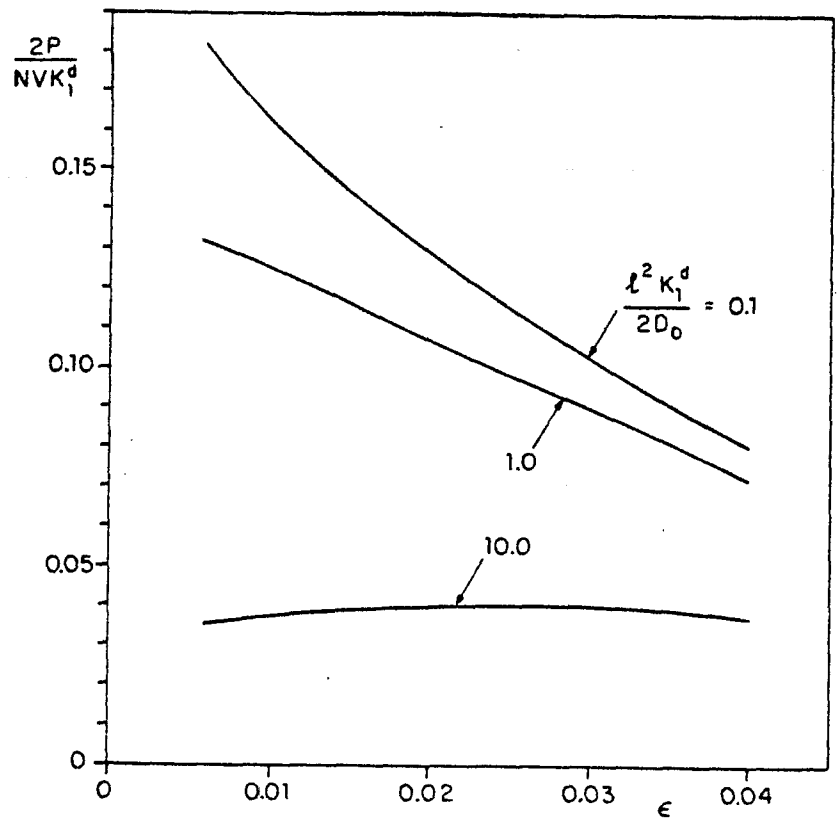

Figure II.8. Steady state permeability as a function of van der Waals cut-off distance ϵ for several values of the dimensionless number $(\ell^2 k_1^d / 2D_0)$ and a transendothelial diffusion distance ℓ of 2500 Å.

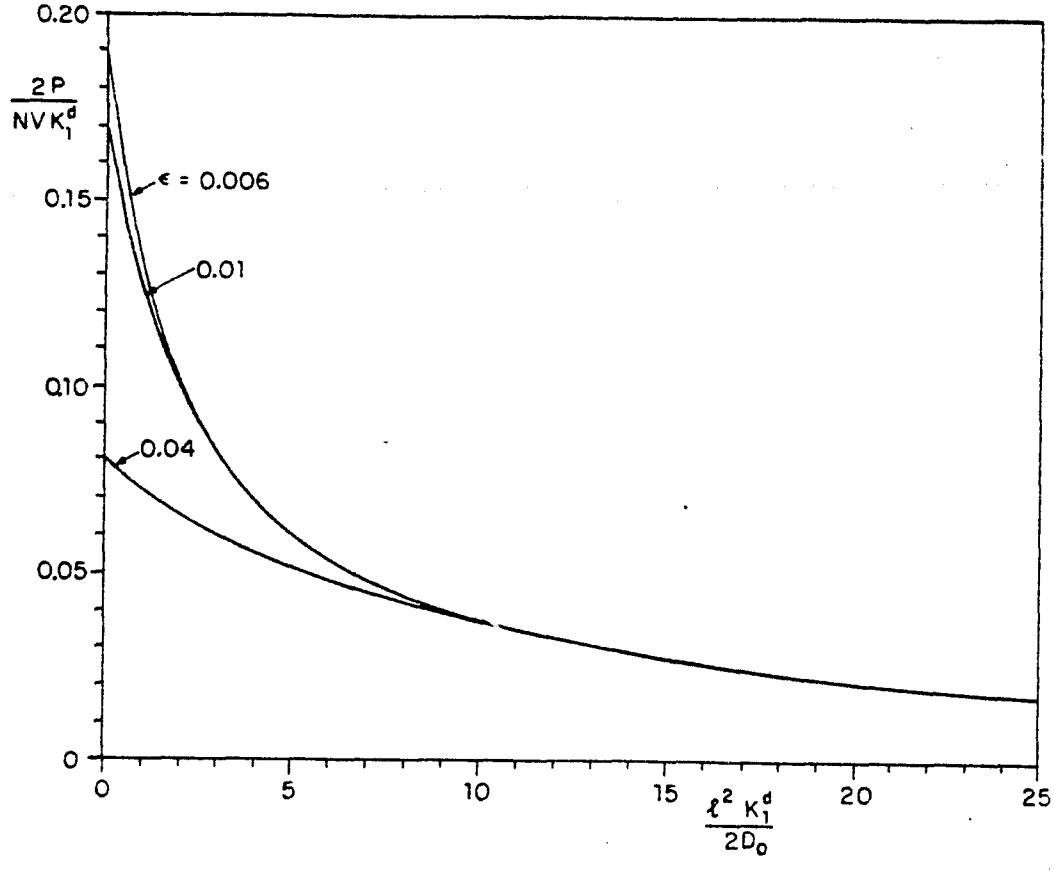

Figure II.9. Steady state permeability as a function of the dimensionless number $(\ell^2 k_1^d / 2D_0)$ for representative values of the effective van der Waals cut-off distance ϵ where the transendothelial diffusion distance ℓ is 2500 Å.

CHAPTER III

STERIC HINDRANCE EFFECTS ON THE TIME DEPENDENT TRANSPORT OF MACROMOLECULES ACROSS VASCULAR ENDOTHELIUM

III-1. INTRODUCTION

In chapter II a time dependent vesicle labelling theory was presented which included the spatial dependence of hydrodynamic and electrodynamic forces produced by both plasmalemma membranes and which was valid for all time. It combined the reaction rate theory of Rubin (1977), modified to take account of the asymmetry of the vesicle attachment/detachment process (Palade and Bruns, 1968) with the spatially non-uniform diffusion theory of Weinbaum and Caro (1976) extended to unsteady one-dimensional diffusion.

In this model a theoretical expression was derived for the spatial variation of the diffusion coefficient, which considered the increased hydrodynamic resistance of a vesicle as it approached the plasma membranes on each side of the endothelial cell, and for the van der Waals electrodynamic attractive force between the vesicle and the boundary plasmalemmas. The agreement of this theory with the steady labelling data of Casley-Smith and Chin (1971) was disappointing although the results for early times were satisfactory. This discrepancy may be due to the steric hindrance of attached vesicles.

All existing theoretical models have neglected the steric hindrance of attached vesicles because there was no available theory or experiment to describe the spatial variation of the vesicle diffusion coefficient as a function of vesicle attachment density. The freeze cleavage

electron micrograph shown in Fig. 2 of Simionescu, Simionescu and Palade (1974) and the extensive data on the density of vesicular openings provide clear evidence that a vesicle attempting to attach at a plasmalemma membrane must experience important steric resistance effects.

It is the purpose of this chapter to determine more realistic expressions for the spatial variation of the vesicle diffusion coefficient and hence obtain an imporved description of transient vesicle dynamics by combining laboratory experiments which model the ultra-structural features of a plasmalemma and its attached vesicles, with the theory of Ganatos, Weinbaum and Pfeffer (1979) for a sphere translating perpendicularly between two parallel walls. Section III-2 is a description of the experimental apparatus and method. In Section III-3 the predictions of the new model, in which experimentally determined values for the hydrodynamic description of the problem are used in conjunction with the theory of chapter II, are presented and discussed.

III-2. EXPERIMENTAL

This section is devoted to a description of the experimental apparatus and method to modify the values of β and θ in expression (II.9) to take account of the steric hindrance behavior in the hydrodynamic resistance parameter λ.

A nylon test sphere measuring 0.5 in. in diameter was dropped through a tube into a rectangular tank filled with UCON 50-HB-5100 fluid. The viscosity of the fluid was such that the Reynolds number was well within the creeping motion range. The test sphere, randomly released, settled under gravity onto an array of identical acrylic spheres which were attached by connecting rods to a plexi-glass plate at the bottom of the tank (see Fig. III.1). The plate and attached spheres were designed to model the ultrastructural features of a plasmalemma membrane and its attached vesicles. The sphere diameter of 0.5 in. corresponded to a vesicle diameter of 700 Å. All other dimensions were scaled according to these figures, including the length of the connecting rod between the plate and attached spheres so that a vesicle neck was simulated.

Three different plates were used each with a different center-to-center spacing between attached spheres. The relationship between center-to-center distance, $\varkappa$, and vesicle number density, ρ, is shown in Fig. III.2. A hexagonal pattern was chosen for the array after carefully viewing the freeze-cleaved preparations of Simionescu, Simionescu and Palade (1974) showing broken vesicle necks

(see for example Fig. 2 in that reference).

The tank was placed on a fatigue mat in order to damp out vibrations. Care was taken to insure the plate was parallel to the surface of the fluid. The experimental set-up was maintained close to 68°F so that the viscosity and density of the fluid were nearly constant. The viscosity was measured using a Brookfield Synchro-lectric LVT viscometer and the density was measured with a constant volume picnometer. Temperature and viscosity measurements were made at the beginning and end of each series of runs to insure that there were no changes in viscosity during the runs and no temperature gradients in the tank.

A Bauer C Royal 6-Zoom Super 8 movie camera was used to take continuous motion pictures of each run. The camera was mounted on a variable-height tripod which was lowered during every run so that the sphere would remain at right angles to the camera not introducing any parallax. In order that a reference scale could be introduced into the picture frame it was decided not to take a direct shot of the falling sphere. Rather, a properly leveled front surface mirror was placed at a distance equidistant to the falling sphere and the reference (ruler). By proper placement a split-screen image was produced. This procedure resulted in a picture of far greater resolution than that of a direct image because the focal length for the images of the sphere and the reference were identical.

A Kodak Ektagraphic MFS-8 movie projector was used to

project the films onto a grid from which measurements were taken. For each 1/8" the sphere traveled, the number of frames on the film were counted. Knowing the number of frames passing per second, velocities at the mean position of the sphere for every 1/8 of an inch were calculated. The ratio of the terminal settling velocity, which was calculated from the physical parameters of the fluid and sphere, over the actual velocity gave the correction to the Stokes drag, λ (hydrodynamic interaction parameter), as a function of distance from the plate, i.e.:

$$\lambda(x) = \frac{u_{ts}}{u(x)} \qquad \text{(III.1)}$$

Here u_{ts} is the terminal settling velocity and u(x) is the measured velocity.

Simionescu, Simionescu and Palade (1974) measured the average density of vesicular openings per μm^2 within the endothelium of both muscular (diaphragm, myocardium) and visceral (pancreas, jejunal villi) capillaries in rats. Their data indicated the number of openings per μm^2 was 78 in diaphragm, 89 in myocardium, 25 in pancreas, and 10 in jejunal mucosa capillaries. Drs. S. Chien and K.M. Jan at the Columbia University School of Medicine have reported numbers of 120 openings per μm^2 in canine carotid artery. On the basis of the above results, spacings of 1100, 1300 and 1500 Å were chosen corresponding to vesicle number densities of 95, 68 and 51 vesicles/μm^2 respectively

as representative values for the experimental runs.

Many spheres were dropped on each plate so that a statistical average for λ could be obtained. All runs were discontinued once the falling sphere touched an attached sphere, thus only hydrodynamic effects were considered.

III-3. RESULTS AND DISCUSSION

Experimentally determined values for the hydrodynamic interaction parameter λ of a sphere settling under gravity onto a plate fitted with an array of identical attached spheres are shown in Fig. III.3 for simulated vesicle center-to-center distances of 1100, 1300 and 1500 Å. These results are shown for increasing distances from the plate as number of sphere radii (x/a).

Below is shown a sample calculation of λ for a simulated vesicle center-to-center distance of 1100 Å. The sphere density ρ_s was measured as 1.104 g/cm^3 and the fluid density $\tilde{\rho}$ was 1.061 g/cm^3. Knowing the viscosity μ of the fluid (2469 cp), the terminal settling velocity was calculated:

$$u_{ts} = \frac{2(\rho_s - \tilde{\rho})g a^2}{9\mu}$$

$$u_{ts} = \frac{2(1.104-1.061)\frac{g}{cm^3} \times 980\frac{cm}{sec^2}\left(\frac{0.5\,in}{2} \times 2.54\frac{cm}{in}\right)^2}{9 \times 2469\,cp \times 1\frac{poise}{cp} \times \frac{1\,g}{cm\text{-}sec/poise}}$$

$$u_{ts} = 0.153\ cm/sec$$

The observed value of the velocity at a distance x/a = 2.57 was 0.0693 cm/sec. Substituting in III.1 gives

$$\lambda = \frac{0.153\ cm/sec}{0.0693\ cm/sec} = 2.2$$

The Reynolds number for this run is also given below:

$$Re = \frac{2 a u_{ts} \tilde{\rho}}{\mu} = \frac{0.5\ in \times 2.54 \frac{cm}{in} \times 0.153 \frac{cm}{sec} \times 1.061 \frac{g}{cm^3}}{2469\ cp \times \frac{1\ poise}{100\ cp} \times \frac{1\ g}{cm\text{-}sec/poise}}$$

$$Re = 0.008$$

Fig. III.3 shows that the vesicle center-to-center spacing χ has an important effect on the hydrodynamic interaction parameter close to the plasmalemma but has little or no influence far away from the plasmalemma. One can see that for small values of x/a, decreasing the vesicle center-to-center distance and hence increasing the steric hindrance due to the steric crowding of attached vesicles significantly increases the correction to the Stokes drag. However, for large values of x/a the value of λ asymptotes to 1.0 for all values of χ.

The results given in Fig. III.3 are valid only for one plasmalemma and its attached vesicles with the second being removed. Close to the plasmalemma, the increased hydrodynamic resistance due to the presence of attached vesicles is so great that the influence of the other plasma membrane can be neglected. But, in the interior part of the cell these experimental values underestimate the value of λ because of the absence of the second wall. Thus, it was decided to use the results of the experiment close to the plasmalemma and the exact solution for a sphere translating perpendicularly between two flat walls (Ganatos, Weinbaum and Pfeffer, 1979) in the interior to estimate λ.

Expression (II.9), with newly determined values of β and θ have been plotted as the solid curves in Figs. III.4, III.5 and III.6 to approximate λ for vesicle center-to-center distances of 1100 Å, 1300 Å and 1500 Å respectively. The transendothelial diffusion distance has been taken as 4300 Å in all of these figures. The new values of β and θ were obtained by a least squares curve fit of the experimental results near the plate and the theoretical results of Ganatos, Weinbaum and Pfeffer (1979), indicated by the dashed curves, in the interior. These values of β and θ are given in Table III.1. The spacing $\alpha = \infty$ in this table corresponds to the case of no steric hindrance. A comparison of the solid and dashed curves in Figs. III.4, III.5 and III.6 shows a significant increase in the value of the hydrodynamic resistance parameter when the effects of steric hindrance are taken into account, especially in the 1100 Å case where the effects of steric hindrance are the greatest.

It is now possible to compare the time dependent vesicle labelling theory developed in chapter II with the tracer studies of Casley-Smith and Chin (1971) using the approximations for λ found above. As in chapter II the comparison is done for an assumed transendothelial diffusion distance of 4300 Å and a van der Waals cut-off distance of 15 Å. The time to reach steady state is taken to be the time at which the peak concentration has reached 98% of its final value.

In Fig. III.7 theoretically predicted concentration

profiles using the values of λ found above are presented, and the experimental data of Casley-Smith and Chin (1971) is also shown. There is a marked improvement over the agreement shown in Fig. II.7. Whereas the agreement in Fig. II.7 was good only for short times, it is very good for all times here.

Using the method described in chapter II to estimate the value of the intracellular viscosity, values of 6.4, 7.8 and 8.5 poise were found for center-to-center distances of 1100, 1300 and 1500 $\mathring{A}$ respectively. All the values were lower, as would be expected, than the value of 8.9 poise found in chapter II where steric exclusion was not considered.

As was mentioned in chapter II if β and ϕ in (II.9) are chosen to be unity, equations (II.50a,b) are identical to steady state solutions (3.25a,b) in Weinbaum and Caro (1976). In Fig. III.8 this solution is compared to the present steady state concentration profile. Fig. III.8 shows better agreement for the new results with the data of Casley-Smith and Chin (1971), especially near the plasmalemma membranes where the effects of steric hindrance are important.

The above concentration profiles show that when steric hindrance is omitted from the hydrodynamic description of the problem the discrepancy between theory and the data of Casley-Smith and Chin (1971) increases. This is clear evidence that steric hindrance is an important factor in the vesicle transport problem. Still, the data of Casley-Smith and Chin must be interpreted cautiously because it

is extremely difficult to distinguish an attached from a free vesicle when close to the plasmalemma if the location of the cutting plane is not known.

In Fig. III.9 the effect of the van der Waals cut-off parameter ϵ_0 is examined. Steady state concentration profiles have been plotted for van der Waals cut-off distances of 15, 50 and 100 Å. The proportion of free labelled vesicles is seen to be higher at the luminal side and lower at the tissue side for the case $\epsilon_0 = 100$ Å than for the smaller van der Waals cut-off distances. This occurs because a vesicle is more likely to reattach at the vesicle plane of release (x=y) the closer ϵ is to x = y. Thus, more labelled vesicles are located near x = y and less are transported across the cell to the tissue side.

One important fact which must be considered is that an incoming vesicle may not be able to fuse directly with a plasma membrane. In a hexagonal pattern the minimum spacing required for a vesicle to just squeeze in is 1212 Å corresponding to a vesicle density of 79 per μm^2. This suggests that incoming vesicles may fuse with already attached vesicles instead of fusing directly with the plasma membrane (Simionescu, Simionescu and Palade, 1974). It is also possible that a vesicle may detach just as another one is attaching. In addition, plasmalemma vesicles, though relatively thick-walled structures (membrane thickness roughly one-fifth of the vesicle

radius), do deform under Brownian motion and thus are capable of penetrating an attached vesicle array that would be impermeable for rigid spheres. These effects were beyond the sophistication of the experiment.

Finally, it should be pointed out that vesicles are not identical. Simionescu, Simionescu and Palade (1974) found a range of 640-720 Å for the diameter of plasmalemma vesicles in rats. In addition there appeared to be areas where the vesicle density was extremely high and no vesicle could fit through, while other areas left enough room for attachment. This non-homogeneity of attached plasmalemma vesicles may have to be considered in future theoretical models as well as laboratory physical model experiments.

In summary, in this chapter the time dependent vesicle labelling theory of chapter II has been modified to include the effects of steric hindrance. When experimentally determined values of the hydrodynamic interaction parameter are included in the theoretical formulation of chapter II, substantially improved agreement with the data of Casley-Smith and Chin (1971) is obtained.

Table III.1. Values of β and θ, including the effects of steric hindrance, in expression (II.9), evaluated by a least squares curve fit of experimentally determined data and the theory of Ganatos, Weinbaum and Pfeffer (1979) for the perpendicular motion of a spherical particle between two plane parallel walls. a = 350 Å, transendothelial diffusion distance = 4300 Å.

x, Å	β	θ
∞	0.9412	1.0504
1500	0.6980	1.7040
1300	0.5735	2.2177
1100	-0.9862	6.6036

CHAPTER III. NOMENCLATURE

a	dimensionless vesicle radius (scaled by trans-endothelial diffusion distance)
a/x	number of vesicle (sphere) radii
c	vesicle number density
c_T	total vesicle number density at any location across endothelial cell
g	gravitational acceleration
$u(x)$	observed velocity as a function of distance above plate
u_{ts}	terminal settling velocity
Re	Reynolds number
x	dimensionless distance coordinate (scaled by transendothelial diffusion distance)
α	vesicle center-to-center distance
y	dimensionless vesicle plane of release (scaled by transendothelial diffusion distance)
β	parameter in correction to Stokes drag
ϵ	dimensionless van der Waals cut-off distance (scaled by transendothelial diffusion distance)
ϵ_0	van der Waals cut-off distance
θ	parameter in correction to Stokes drag
$\lambda(x)$	hydrodynamic interaction parameter as a function of position
μ	fluid viscosity
ρ	number of vesicles per μm^2
ρ_s	particle (sphere) density
$\tilde{\rho}$	fluid density

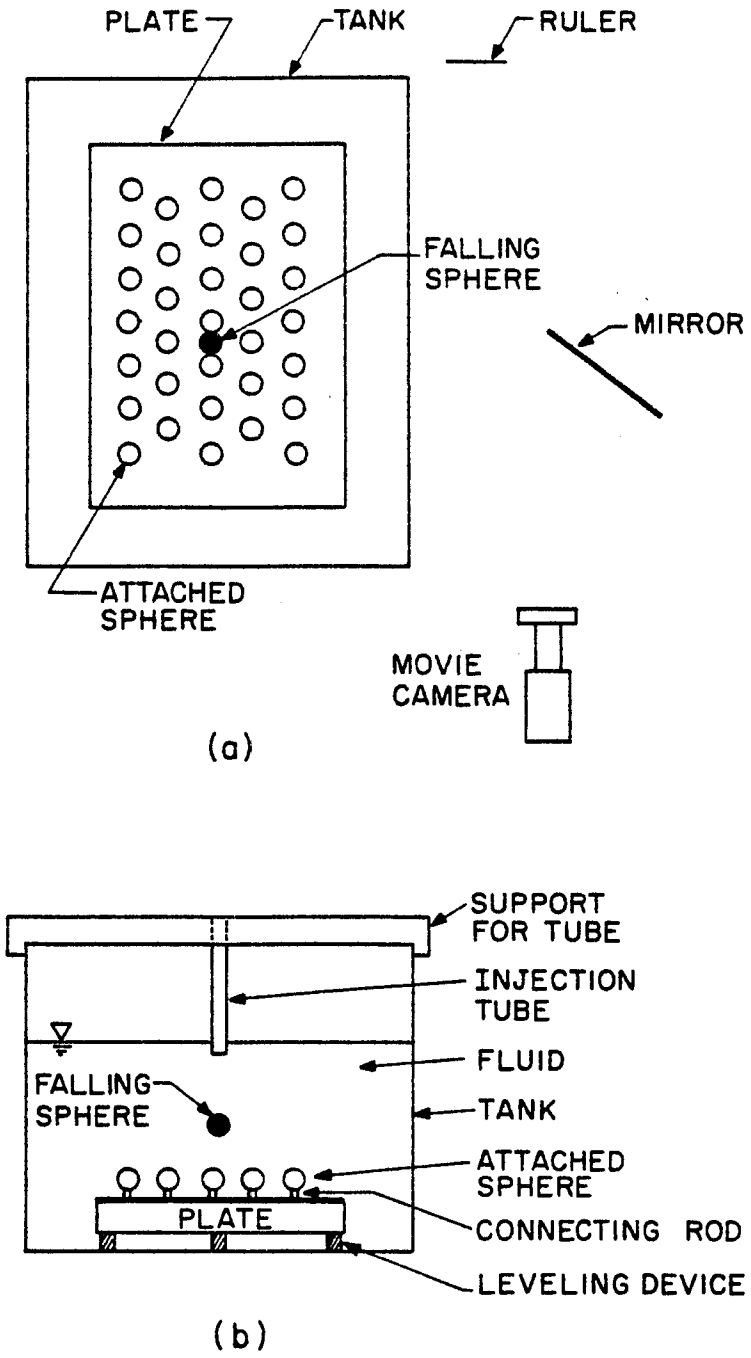

Figure III.1. Schematic illustration of experimental apparatus. (a) Top view of tank with tube support removed, ruler, mirror and movie camera. (b) Front view of tank.

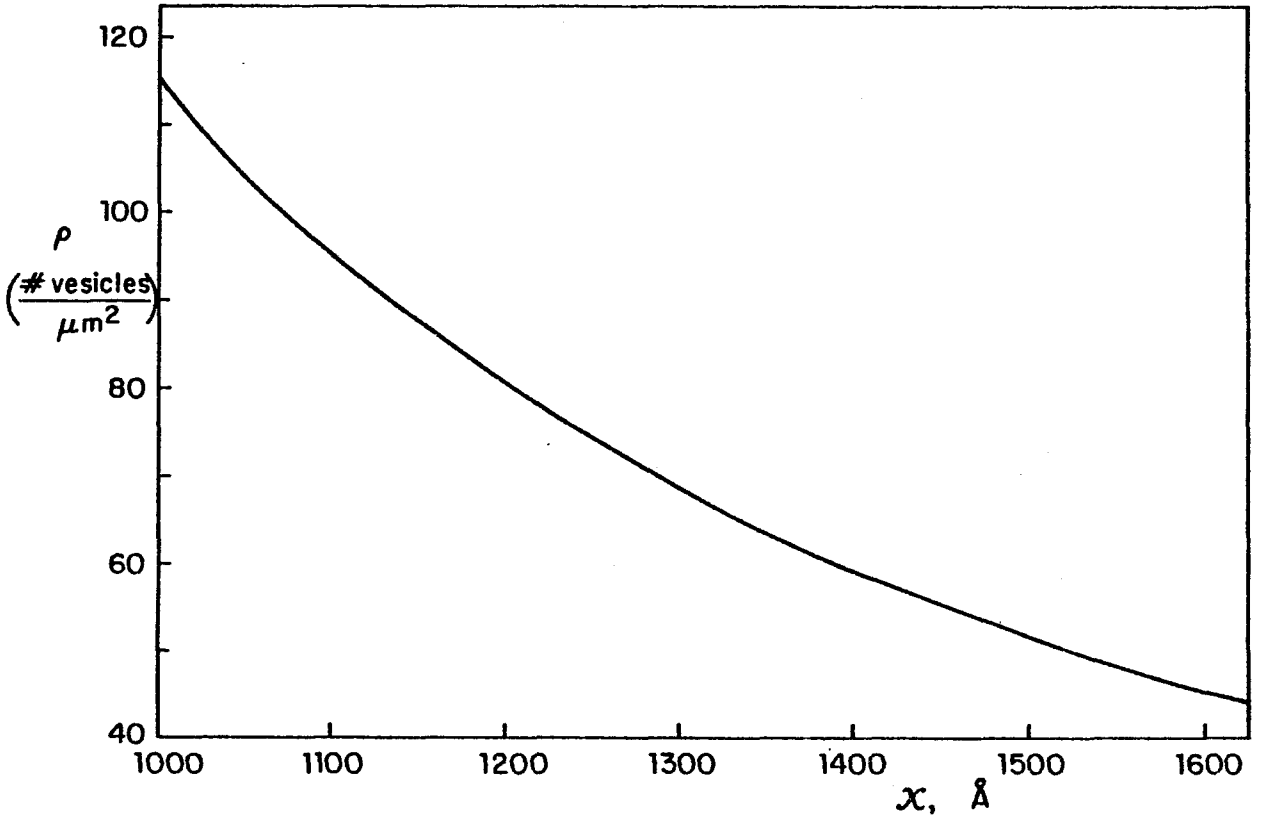

Figure III.2. Vesicle density per μm^2 ρ as a function of vesicle center-to-center distance x in a hexagonal array.

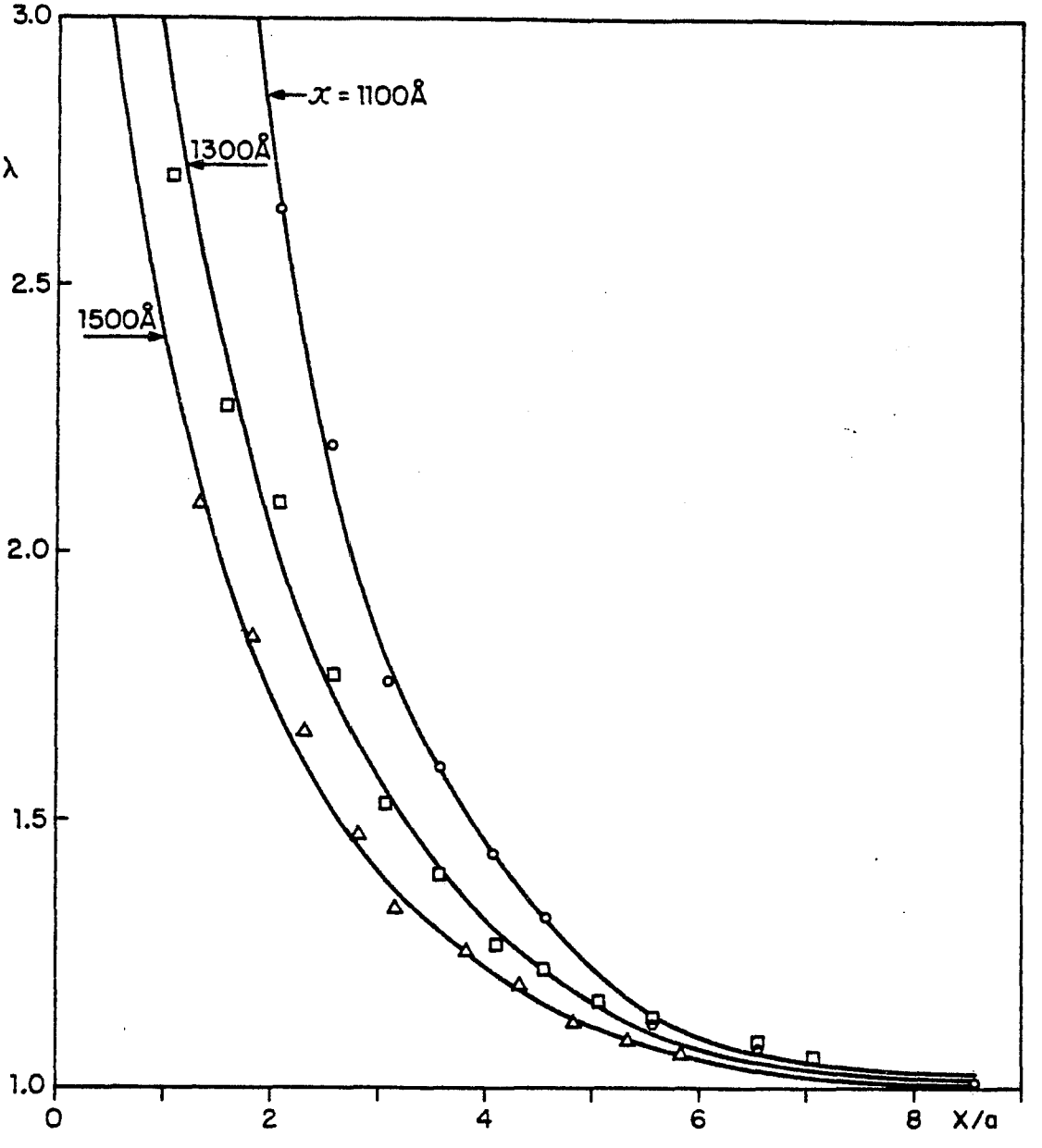

Figure III.3. Correction to Stokes drag as a function of number of vesicle radii (x/a) from plasma membrane for various vesicle center-to-center, $\varkappa$, distances. Experimental data: o - $\varkappa$ = 1100 Å; □ - $\varkappa$ = 1300 Å; △ - $\varkappa$ = 1500 Å.

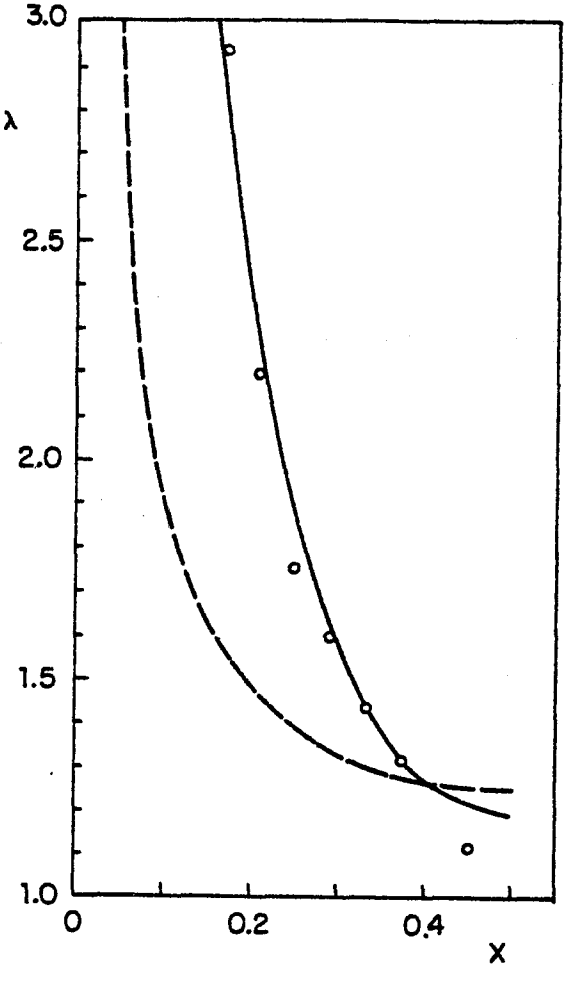

Figure III.4. Correction to Stokes drag across endothelial cell for a vesicle center-to-center distance of 1100 Å and a transendothelial diffusion distance of 4300 Å. o - experimental data; ---- theory of Ganatos, Weinbaum and Pfeffer (1979); —— curve fit.

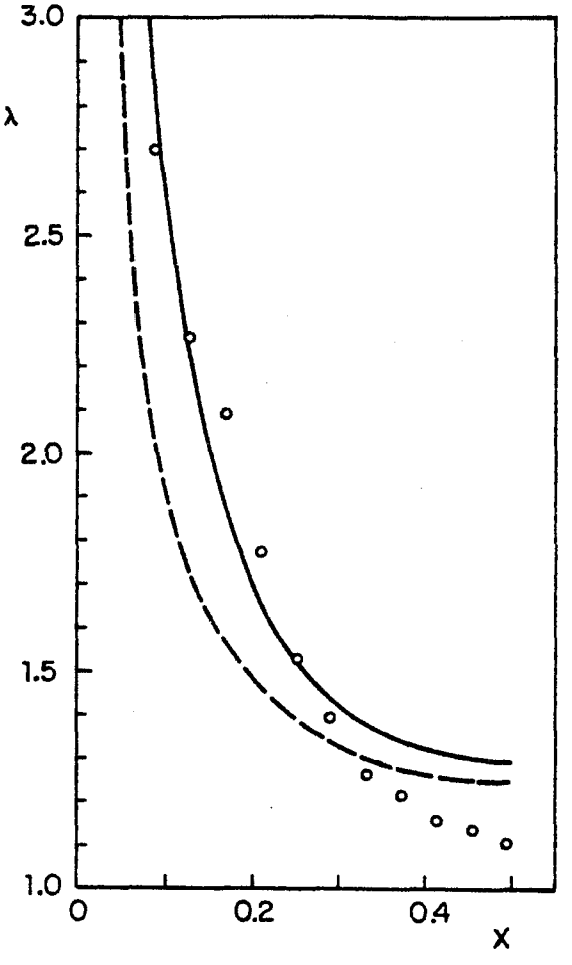

Figure III.5. Correction to Stokes drag across endothelial cell for a vesicle center-to-center distance of 1300 Å and a transendothelial diffusion distance of 4300 Å. o - experimental data; ---- theory of Ganatos, Weinbaum and Pfeffer (1979); —— curve fit.

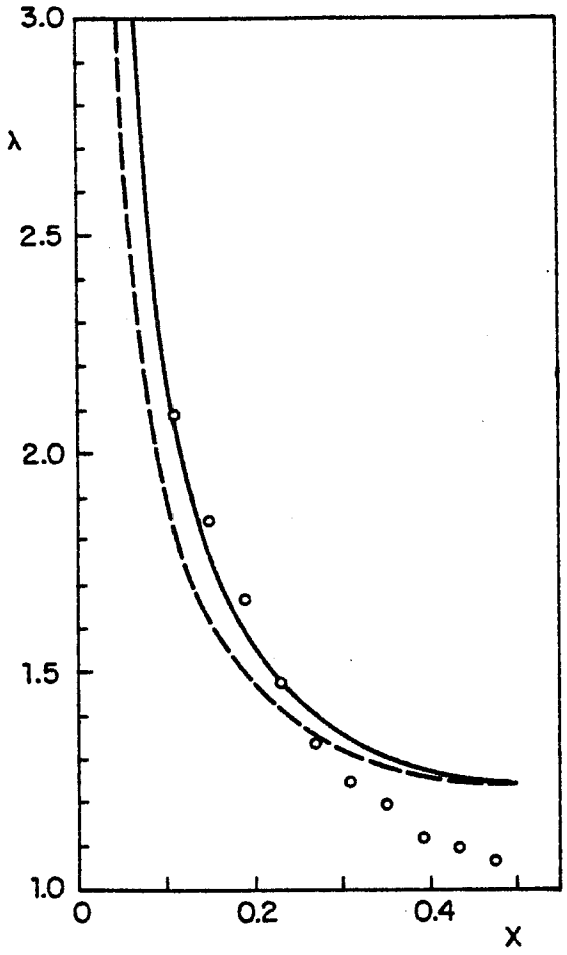

Figure III.6. Correction to Stokes drag across endothelial cell for a vesicle center-to-center distance of 1500 Å and a transendothelial diffusion distance of 4300 Å. o - experimental data; ---- theory of Ganatos, Weinbaum and Pfeffer (1979); —— curve fit.

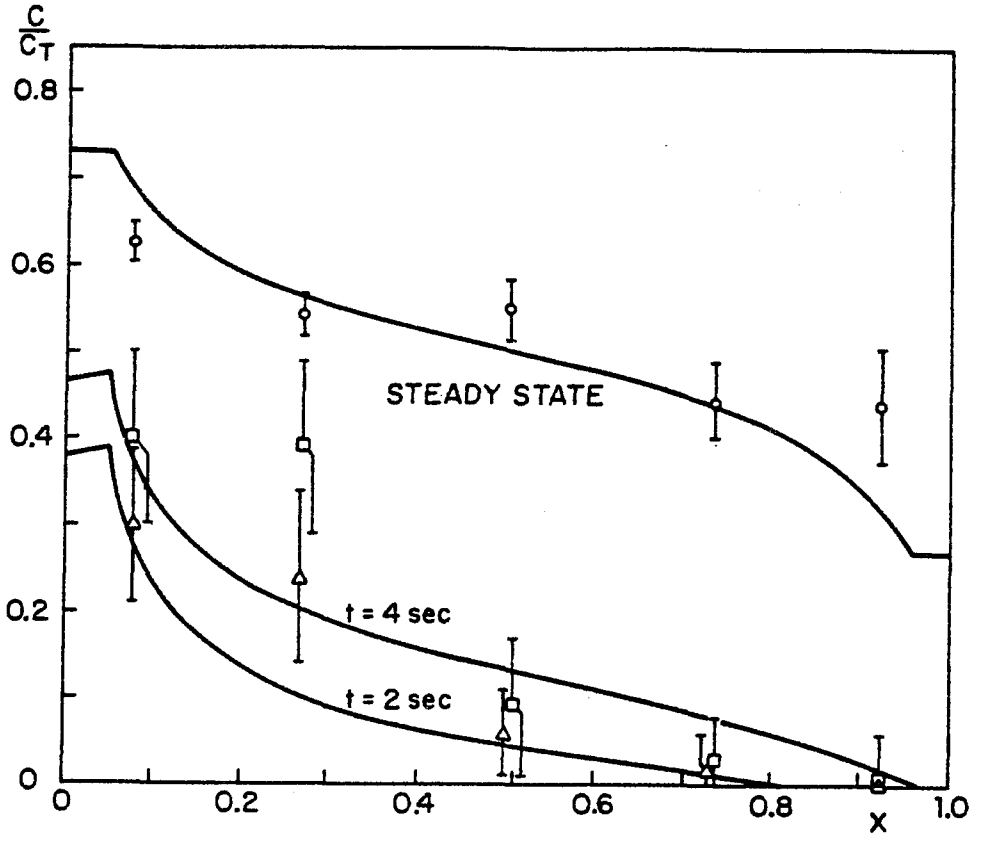

Figure III.7. Theoretical and experimental time dependent proportion of labeled vesicles c/c_T as a function of distance x for an effective van der Waals cut-off distance of 15 Å, a trans-endothelial diffusion distance of 4300 Å and a vesicle center-to-center distance $\mathscr{x}$ of 1100 Å. Experimental data, Δ , 2s; $\square$, 4s; o $\geq$ 16s (Casley-Smith and Chin, 1971: vesicles labeled with horseradish peroxidase). Vertical bars represent ± 1 standard error.

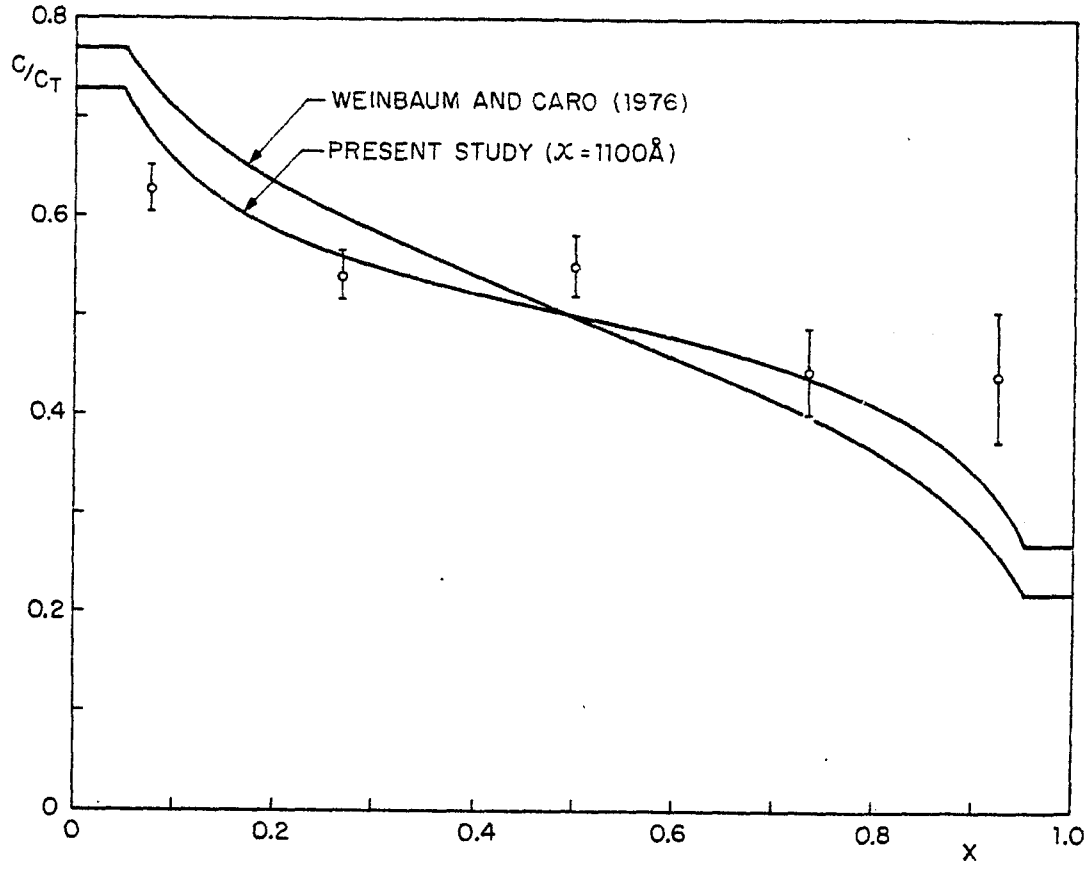

Figure III.8. Comparison of steady state proportion of labeled vesicles c/c_T as a function of distance x of Weinbaum and Caro[1](1976) and present study ($\varkappa$ = 1100 Å) for an effective van der Waals cut-off distance ϵ_0 of 15 Å and a transendothelial diffusion distance of 4300 Å. Experimental data, o ≥ 16s (Casley-Smith and Chin, 1971: vesicles labeled with horseradish peroxidase). Vertical bars represent ±1 standard error.

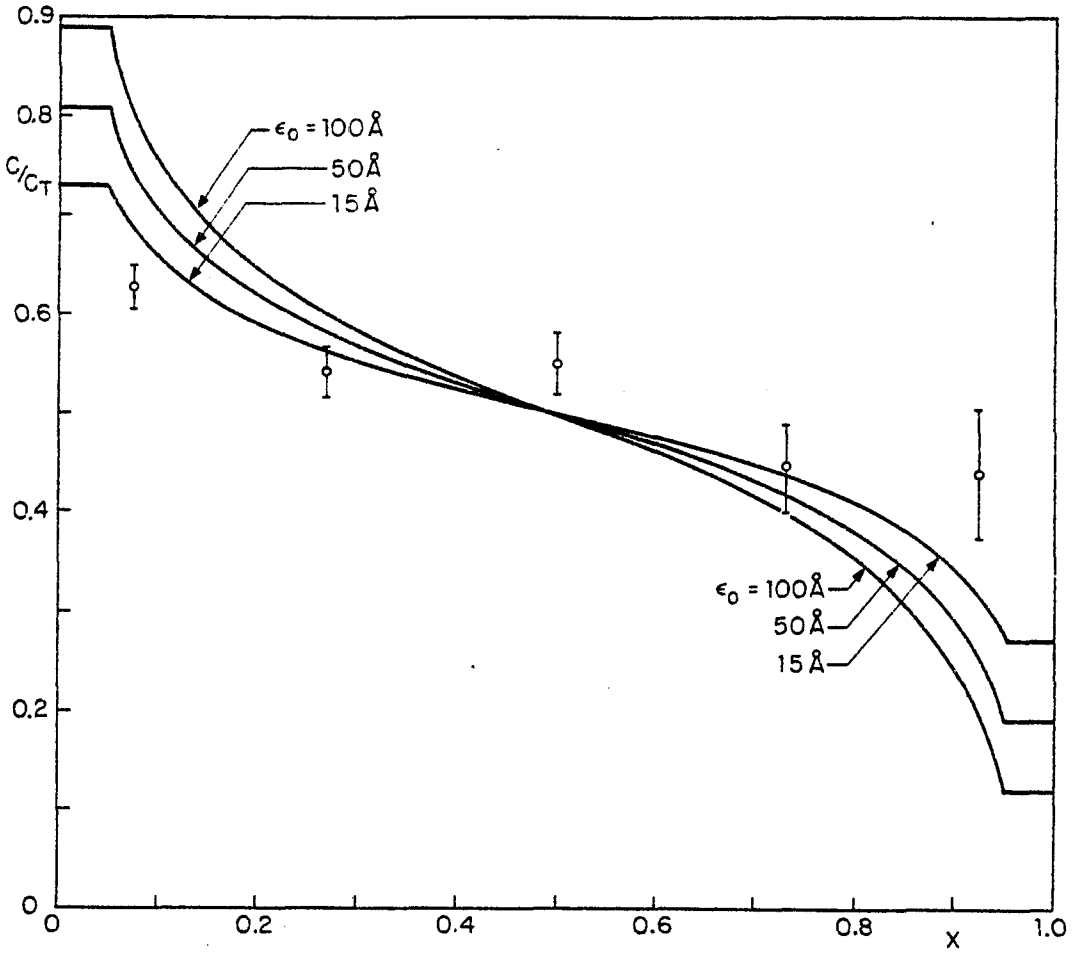

Figure III.9. Effect of van der Waals cut-off parameter ϵ_0 on steady state proportion of labeled vesicles c/c_T as a function of distance x for a transendothelial diffusion distance of 4300 Å and a vesicle center-to-center distance $\varkappa$ of 1100 Å. Experimental data, $o \geq 16s$ (Casley-Smith and Chin, 1971: vesicles labeled with horseradish peroxidase). Vertical bars represent ± 1 standard error.

REFERENCES

Alder, B.J. and Wainwright, T.E. 1967 Phys. Rev. Lett. 18, 988.

Alder, B.J. and Wainwright, T.E. 1968 J. Phys. Soc. Jpn. Suppl. 26, 267.

Alder, B.J. and Wainwright, T.E. 1970 Phys. Rev. A1, 18.

Basset, A.B. 1888 Trans. R. Soc. London A179, 43.

Basset, A.B. 1910 Quart. J. Math. 41, 369.

Batchelor, G.K. 1976 Theoretical and Applied Mechanics (ed. W.T. Koiter), p. 36., North-Holland, Amsterdam.

Berne, B.J. 1971 Physical Chemistry: an Advanced Treatise (ed. D. Henderson), Vol. VIIIB, Chap. 9, Academic, New York.

Boggio, T. 1907 Rendiconti della R. Accad. dei Lincei 16, series 5.

Bruns, R.R. and Palade, G.E. 1968 J. Cell Biol. 37, 277.

Caro, C.G. 1978 Specialists Meeting at the Ohio State University, Columbus, Ohio, August 24-25, 1978.

Casley-Smith, J.R. and Chin, J.C. 1971 J. Microsc. 93, 167.

Clough, G. and Michel, C.C. 1978 Proc. Physiol. Soc. C.56, 95P.

Corrsin, S. and Lumley, J. 1956 Appl. Sci. Res. A6, 114.

Cox, R.G. and Brenner, H. 1968 Chem. Engng. Sci. 22, 1753.

Einstein, A. 1905 Ann. Phys. (Leipzig) 17, 549.

Fry, D.L. 1972 Circul. Res. 24, 93.

Ganatos, P., Weinbaum, S. and Pfeffer, R. 1979 Submitted for publication.

Glasstone, S., Laidler, K.J. and Eyring, H. 1941 The Theory of Rate Processes, pp. 1-28., 516-525., McGraw-Hill, New York.

Green, H.S. and Casley-Smith, J.R. 1972 J. Theor. Biol. 35, 103.

Hinch, E.J. 1975 J. Fluid Mech. 72, 499.

Hinze, J.O. 1975 Turbulence, p. 460., McGraw-Hill, New York.

Ho, B.P. and Leal, L.G. 1974 J. Fluid Mech. 65, 365.

Israelachvili, J.N. and Tabor, D. 1972 Prog. Surface Membrane Sci. 7, 1.

Karnovsky, M.J. 1967 J. Cell Biol. 37, 213.

Kubo, R. 1966 Rept. Progr. Phys. 29, 235.

Landau, L.D. and Lifshitz, E.M. 1959 Fluid Mechanics, p. 96., Pergamon, New York.

Lightfoot, E.N. 1974 Transport Phenomena and Living Systems, pp. 113-120., John Wiley and Sons, New York.

Lodish, H.F. and Rothman, J.E. 1979 Sci. Am. 240, 48.

Newman, H.A.I. and Zilversmit, D.B. 1966 Circ. Res. 18, 293.

Palade, G.E. 1960 Anat. Record 136, 245.

Palade, G.E. and Bruns, R.R. 1968 J. Cell Biol. 37, 633.

Parsegian, V.A. 1973 Ann. Rev. Biophys. Bioeng. 2, 221.

Picciati, G. 1907 Rendiconti della R. Accad. dei Lincei 16, series 5.

Rubin, B.T. 1977 J. Theor. Biol. 64, 619.

Shea, S.M. and Bossert, W.H. 1973 Microvasc. Res. 6, 305.

Shea, S.M., Karnovsky, M.J. and Bossert, W.H. 1969 J. Theor. Biol. 24, 30.

Siflinger, A., Parker, K. and Caro, C.G. 1975 Cardiovasc. Res. 9, 478.

Simionescu, N., Simionescu, M. and Palade, G.E. 1973 J. Cell Biol. 57, 434.

Simionescu, M., Simionescu, N. and Palade, G.E. 1974 J. Cell Biol. 60, 128.

Simionescu, N., Simionescu, M. and Palade, G.E. 1975 J. Cell Biol. 64, 586.

Simionescu, M., Simionescu, N. and Palade, G.E. 1976 J. Cell Biol. 68, 705.

Tchen, C.M. 1947 Doctoral thesis, Technical University, Delft, Netherlands.

Tomlin, S.G. 1969 Biochem. Biophys. Acta 183, 559.

Villat, H. 1943 Lecons sur les Fluides Visqueux, p. 218., Gauthier-Villars, Paris.

Weinbaum, S. 1979 J. Theor. Biol. In press.

Weinbaum, S. and Caro, C.G. 1976 J. Fluid Mech. 74, 611.

Widom, A. 1971 Phys. Rev. A3, 1394.

Yih, C.S. 1969 Fluid Mechanics, p. 375., McGraw-Hill, New York.

Zwanzig, R. and Bixon, M. 1970 Phys. Rev. A2, 2005.